J. Fluid Mech. (1992), *vol.* 239, *pp.* 213–248
Printed in Great Britain

Measurements of the streamwise vortical structures in a plane mixing layer

By JAMES H. BELL AND RABINDRA D. MEHTA

Mail Stop 260-1, Fluid Mechanics Laboratory, Fluid Dynamics Research Branch, NASA Ames Research Center, Moffett Field, CA 94035, USA *and* Department of Aeronautics and Astronautics, JIAA, Stanford University, Stanford, CA 94305, USA

(Received 3 May 1991 and in revised form 4 December 1991)

An experimental study has been conducted to investigate the three-dimensional structure of a plane, two-stream mixing layer through direct measurements. A secondary streamwise vortex structure has been shown to ride among the primary spanwise vortices in past flow visualization investigations. The main objective of the present study was to establish *quantitatively* the presence and role of the streamwise vortex structure in the development of a plane turbulent mixing layer at relatively high Reynolds numbers ($Re_\delta \sim 2.9 \times 10^4$). A two-stream mixing layer with a velocity ratio, $U_2/U_1 = 0.6$ was generated with the initial boundary layers laminar and nominally two-dimensional. Mean flow and turbulence measurements were made on fine cross-plane grids across the mixing layer at several streamwise locations with a single rotatable cross-wire probe. The results indicate that the instability, leading to the formation of streamwise vortices, is initially amplified just downstream of the first spanwise roll-up. The streamwise vortices first appear in clusters containing vorticity of both signs. Further downstream, the vortices re-align to form counter-rotating pairs, although there is a relatively large variation in the scale and strengths of the individual vortices. The streamwise vortex spacing increases in a step-wise fashion, at least partially through the amalgamation of like-sign vortices. For the flow conditions investigated, the wavelength associated with the streamwise vortices scales with the mixing-layer vorticity thickness, while their mean strength decays as approximately $1/X^{1.5}$. In the near field, the streamwise vortices grossly distort the mean velocity and turbulence distributions within the mixing layer. In particular, the streamwise vorticity is found to be strongly correlated in position, strength and scale with the secondary shear stress ($\overline{u'w'}$). The secondary shear stress data suggest that the streamwise structures persist through to what would normally be considered the self-similar region, although they are very weak by this point and the mixing layer otherwise appears to be two-dimensional.

1. Introduction

Turbulent mixing layers have been a popular subject of study for many years, not only because of their importance in practical aerodynamics, but also due to their fundamental importance in the study of free-shear flows. In practical applications, mixing layers govern the rate of mixing in combustion chambers and flow reactors, and are also responsible for most of the broadband noise generated in propulsion systems. The ability to control the mixing, structure and growth of this shear flow would obviously have a vital impact on many engineering applications. The

structure of plane mixing layers also exhibits certain unique features which have made them attractive for fundamental experimental and computational studies.

The idea of organized or 'coherent' structures existing in turbulent shear flows was first introduced in the form of a large-eddy hypothesis by Townsend (1956). Freymuth (1966) and Winant & Browand (1974) later observed the formation and pairing of mixing-layer structures in the form of concentrated spanwise vortices. Brown & Roshko's (1974) results created renewed excitement since they reported that their spanwise vortical structures were two-dimensional and that they persisted into the self-similar region, even at very high Reynolds numbers. Experimental research in this area was at once revived and many of the subsequent studies concentrated on the search for, and characterization of, the coherent structures (see Cantwell 1981 and Ho & Huerre 1984 for reviews). While many researchers reported the presence of large-scale structures in mixing layers, there was considerable disagreement regarding the spanwise coherence of the structures and their persistence into the far-field region (Chandrsuda *et al.* 1978; Bradshaw 1979). In the meantime, the presence of an organized secondary structure, in the form of *streamwise* vorticity, was also becoming apparent.

The presence of streamwise vortices in mixing layers was reported as early as 1966 by Bradshaw, who mentioned that flow visualization studies (Bradshaw, Ferriss & Johnson 1964) had shown their appearance just prior to the breakdown of an axisymmetric mixing layer to a fully turbulent state. However, the first real investigation of this phenomenon was performed by Konrad (1976), who observed streamwise streaks in plan-view shadowgraphs of the mixing layer produced in Brown & Roshko's (1974) apparatus. Konrad concluded that the streaks were evidence of a series of hairpin vortices, oriented in the streamwise direction and lying between adjacent spanwise vortices. The appearance of the streaks was correlated with a sudden increase in mixing observed in concentration measurements, which Konrad called 'mixing transition'. Breidenthal (1978, 1981) used a water tunnel to repeat Konrad's mixing study at a higher Schmidt number so as to better resolve the mixing transition. He also observed a row of streamwise streaks in the mixing layer, which he found to originate in 'wrinkles' in the spanwise vortices. Again, the appearance of the streaks was correlated with the location of mixing transition. Further details of the streamwise structure were provided by Jimenez (1983) in his study of a half-jet. His streamwise velocity contour plots showed a well-defined and steady spanwise disturbance, consisting of wrinkles whose wavelength increased with downstream distance. Later, Jimenez, Cogollos & Bernal (1985) used digital image processing to construct three-dimensional models of mixing-layer structures from the flow visualization data of Bernal (1981). Based on these models, Jimenez *et al.* suggested that the streamwise vorticity first originated in the *braid* region which connects adjacent spanwise vortex cores. The picture of the streamwise structure as a single row of alternating-sign vortices was firmly established at high Reynolds numbers ($Re_{\delta_\omega} = 40000$, where δ_ω is the mixing-layer vorticity thickness) by Bernal & Roshko (1986), and at low Reynolds numbers ($Re_{\delta_\omega} = 500$) by Lasheras, Cho & Maxworthy (1986). The latter study, together with that of Lasheras & Choi (1988), elucidated the initial development of the streamwise vortex structure. It was found that although the location of the initial appearance of the vorticity varied from one flow visualization to the next, it always occurred in the braid region. The streamwise structures, of scale somewhat smaller than the spanwise ones, then propagated into the spanwise vortex cores. Further analysis showed that the streamwise vortices were grouped into closely spaced pairs of counter-rotating vortices, with somewhat

more space between pairs than between the vortices within each pair. Lasheras *et al.* (1986) suggested that the streamwise vortices were a result of 'an unstable response of the layer to three-dimensional perturbations in the upstream conditions'. This hypothesis was confirmed by triggering the vortices using small periodic perturbations along the splitter plate trailing edge (Lasheras & Choi 1988).

The experimental studies, particularly those of Bernal & Roshko (1986), Lasheras *et al.* (1986) and Lasheras & Choi (1988), are consistent with analyses of the stability of the mixing layer to spanwise perturbations (Corcos & Sherman 1984; Corcos & Lin 1984; Lin & Corcos 1984). Together, these studies have led to a widely accepted picture of the streamwise vortex structure. The structure is believed to arise in the braid region where residual spanwise vorticity is stretched by the strain field produced by the spanwise structures. The extensional principle axis of the strain field is along a line perpendicular to the spanwise direction, and is oriented at an angle to the streamwise direction. The result is the formation of a vortex tube which winds back and forth between adjacent spanwise rollers. When viewed from above, this structure appears to be a row of alternating-sign streamwise vortices embedded in the mixing layer. This picture of the structure has also been observed in results of temporal numerical simulations using both the vortex tracking approach (Ashurst & Meiberg 1988) and the direct Navier–Stokes method (Metcalfe *et al.* 1987; Rogers & Moser 1989).

In addition to the instability mechanism proposed by Corcos *et al.*, researchers have also noted instability modes in the spanwise vortices themselves which can lead to the production of organized streamwise vorticity. Pierrehumbert & Widnall (1982) modelled the spanwise structures as an array of Stuart vortices and found two types of three-dimensional instabilities. The first is a slowly growing antisymmetric mode which may be responsible for the observed helical (Chandrsuda *et al.* 1978) and irregular (Browand & Troutt 1985) spanwise vortex pairing. The symmetric mode results in an undulation of the spanwise vortex core, thus forming a pattern of alternating-sign streamwise vorticity directly from the spanwise vortices. This behaviour has been observed in recent flow visualization studies by Nygaard & Glezer (1990) who used spatially and temporally varying heating elements to excite the proper instability modes. The importance of these instability modes will be in determining the details of the interaction between the streamwise and spanwise structures.

While the results from the various investigations do not agree in all areas, there is some consensus regarding the initial development of the streamwise vortical structures. Organized streamwise vortices have been observed experimentally in the near field of mixing layers developing from *untripped* initial boundary layers which in most cases were shown to be in a laminar state. To our knowledge, organized (spatially stationary) streamwise vorticity has not been observed in mixing layers originating from turbulent boundary layers (Bell & Mehta 1990*b*). The downstream location at which significant streamwise vorticity first appears has been found to be very sensitive to initial conditions (Lasheras *et al.* 1986). Konrad (1976), Breidenthal (1978), and Bernal & Roshko (1986) have all argued that the streamwise location of appearance depends on Reynolds number, with Bernal & Roshko finding a dependence on velocity ratio as well. Unfortunately, since the various flow visualization techniques have differing thresholds at which vorticity first becomes 'visible', it is difficult to compare the results from different studies directly. In most cases, though, the streamwise vortices were first observed in the braid region

connecting the spanwise vortical structures (Jimenez *et al.* 1985; Lasheras *et al.* 1986).

Streamwise vortex structures seem to first appear at spatially fixed, but irregular spanwise locations for a given set of wind tunnel conditions (Jimenez 1983). Bernal & Roshko (1986) and Jimenez (1983) found that the lateral locations at which the streamwise vortices first appeared could be altered by changing the flow conditions on the splitter plate, thus suggesting that upstream disturbances play a crucial role in triggering the streamwise vortices. Lasheras *et al.* point out that, according to the model of Corcos &Lin (1984), one streamwise structure will tend to generate similar structures on either side, resulting in a lateral spread of the streamwise vortex structure. The results of Lasheras *et al.* and Bernal & Roshko are consistent with this picture – small disturbances in the upstream boundary layer trigger the amplification of a streamwise structure, which spreads laterally to fill the mixing layer.

Lasheras & Choi (1988) applied a known spanwise disturbance to their mixing layer using several differently sized corrugated splitter plates. The resulting streamwise structures were locked to the corrugation over a broad range of wavelengths, with no obvious sign of a most-amplified wavelength. Stability analyses (Pierrehumbert & Widnall 1982; Ho *et al.* 1988) suggest that the mixing layer will amplify spanwise disturbances more-or-less equally over a broad range of wavelengths, with the most-amplified wavelength being about $\frac{2}{3}$ of the Kelvin–Helmholtz wavelength. This is consistent with several previous experimental studies (Konrad 1976; Breidenthal 1978; Jimenez 1983; Jimenez *et al.* 1985; Bernal & Roshko 1986; Lasheras *et al.* 1986; Huang & Ho 1990), which all report that the initial average wavelength is of the same order of magnitude as the Kelvin–Helmholtz wavelength.

There is some disagreement on the subsequent evolution of the streamwise structures. The flow visualizations of Breidenthal (1978), Lasheras *et al.* (1986), and Lasheras & Cho (1988) show no change in spanwise wavelength with downstream distance. In contrast, Konrad, Jimenez, and Jimenez *et al.* show the spanwise wavelength changing in a stepwise fashion. Significantly, the flow visualization results of Jimenez *et al.* (1985) show the streamwise vortex wavelength doubling during a pairing of the spanwise vortices, a result which was recently confirmed in the measurements due to Huang & Ho (1990). One possible mechanism by which the wavelength may increase during pairing was proposed by Martel, Mora & Jimenez (1989) and Rogers & Moser (1989). Briefly, conservation of energy and momentum during spanwise vortex pairing requires that some spanwise vorticity be 'thrown out' into the braids, recapitulating the process which occurs during the initial roll-up, but with a doubled spanwise instability wavelength. Thus, the streamwise vortex structure is created anew, with twice the previous wavelength. In a realistic mixing layer, where irregular vortex pairing occurs, as well as such phenomena as vortex tearing and multiple vortex interactions (Polinsky 1989), the streamwise wavelength might be expected to grow linearly, at a rate corresponding to the mixing-layer growth rate. In fact, the measurements of Jimenez (1983) show that the wavelength scales as approximately $1.0\text{–}1.25 \times \delta_\omega$. Similarly, Bernal & Roshko's (1986) flow visualizations show that (after an initial region of constant wavelength) the streamwise vortex wavelength increases linearly, as approximately $0.8\delta_\omega$.

Previous estimates of the strength of the streamwise vorticity have been the product of a long chain of analytical reasoning, but surprisingly have given similar results. Jimenez (1983) calculated that the streamwise vortex circulation was equivalent to between 1 and 1.5 times that of the initial spanwise circulation in the

Kelvin–Helmholtz roll-up. This estimate was based on the thickness of the mixing layer and the extent of distortion in the mean velocity contours which the streamwise structures produced. Using a completely unrelated approach, which assumed that the streamwise structures were a regular array of counter-rotating vortices, Jimenez *et al.* (1985) estimated the streamwise to spanwise circulation ratio to be about 1.6. O'Hern (1990) modelled the streamwise vortices as Rankine vortices, in a high-speed cavitation flow study, and estimated the streamwise vortex circulation to be comparable to the initial spanwise circulation.

There is some disagreement as to how much effect the streamwise vortices have on the mixing layer. The photos of Lasheras & Choi (1988) show no effect on the gross structure of the dominant spanwise vortices. On the other hand, large spanwise variations are noted in the mean velocity measurements (Jimenez 1983; Huang & Ho 1990), implying significant effects on momentum transport. In addition, the concentration measurements of Konrad (1976) and Breidenthal (1978) suggest that streamwise vorticity can have a considerable effect on scalar transport, thus affecting mixing between the two streams.

While a considerable amount of work has already been conducted on the three-dimensional structure of mixing layers, many areas of confusion still remain regarding the origin, evolution and development of the streamwise vortices. Further *direct and quantitative* data on the streamwise vortex structure are needed before these issues can be fully resolved. Accordingly, the objectives of the present study were to investigate the origin of the streamwise vortex structure and characterize its development, particularly its changes in scale and strength as the mixing layer grows, extending into the far-field, self-similar region. The effects of the streamwise vortex structure on the mean flow and turbulence statistics of the mixing layer were also to be investigated. Some of the more important results are presented in this paper; full details of the investigation are given in Bell & Mehta (1989*a*).

2. Experimental apparatus and techniques

The experiments were conducted in a specially designed mixing-layer wind tunnel (figure 1), consisting of two separate legs which are driven individually by centrifugal blowers connected to variable-speed motors. Downstream of the wide angle diffusers, the wind tunnel legs are mirror images of each other, with similar flow conditioning elements installed on both sides. The two streams are allowed to merge at the sharp trailing edge of a tapered splitter plate. The included angle at the splitter plate edge, which extends 15 cm into the test section, is about 1°, and the edge thickness is approximately 0.25 mm. The test section is 36 cm in the cross-stream direction, 91 cm in the spanwise direction and 366 cm in length. One sidewall is slotted for probe access and also flexible for pressure gradient control. For all of the present measurements, the flexible wall was adjusted to give a nominally zero streamwise pressure gradient; the streamwise variation in static pressure was less than 1% of the dynamic head in the test section.

For the present experiments, the leg driven by the bigger blower was operated at a free-stream velocity in the test section of 15 m/s whereas the other leg was run at 9 m/s, thus giving a mixing layer with velocity ratios, $r = U_2/U_1 = 0.6$ and $\lambda = [(1-r)/(1+r)] = 0.25$. The free-stream velocities were held constant to within 1% during a typical run lasting two hours. At these operating conditions, the measured streamwise turbulence intensity level (u'/U_e) in the free-stream was about 0.15% and the transverse levels (v'/U_e and w'/U_e) were about 0.05%. The mean core

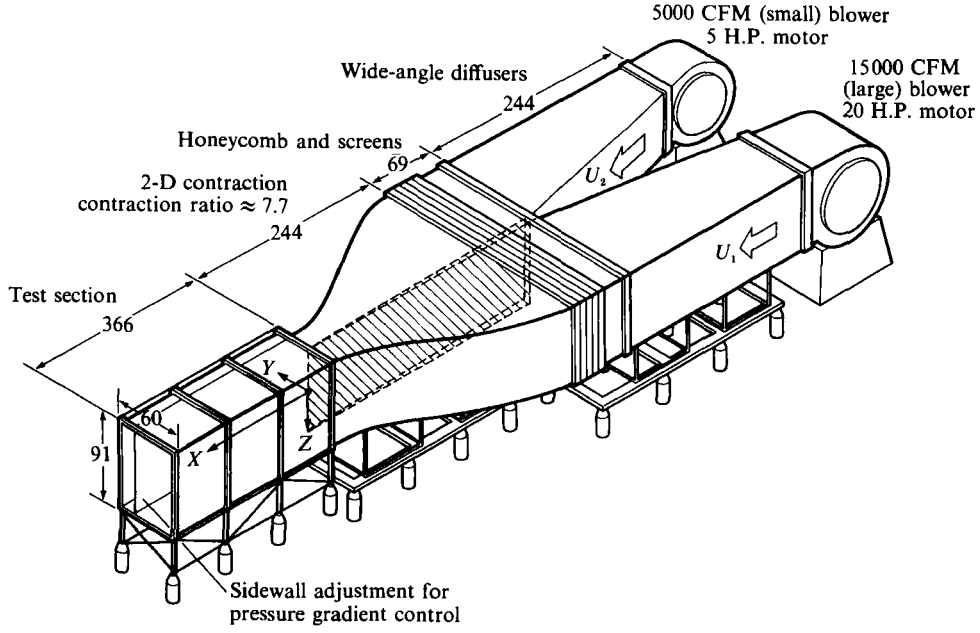

FIGURE 1. Schematic of mixing-layer wind tunnel. Dimensions in cm.

Side	U_e (m/s)	δ_{99} (cm)	θ (cm)	Re_θ	H
High-speed	15.0	0.40	0.053	525	2.52
Low-speed	9.0	0.44	0.061	362	2.24

TABLE 1. Initial boundary-layer properties

flow was found to be uniform to within 0.5% and cross-flow angles were less than 0.25°. Further details of the wind tunnel design and flow quality measurements are given in Bell & Mehta (1989*b*). Details of the laminar boundary layers, averaged over five spanwise locations at the trailing edge of the splitter plate, are given in table 1. The boundary layers were found to be adequately two-dimensional with the properties given above varying by less than 2% across the splitter plate span.

The main measurements were made using a cross-wire probe held on a three-dimensional traverse and linked to a fully automated data acquisition and reduction system controlled by a MicroVax II computer. The cross-wire probe had 5 μm tungsten sensing elements about 1 mm long and positioned about 1 mm apart. The probe was calibrated statically in the potential core of the flow (between the mixing layer and the wall boundary layer) assuming a 'cosine-law' response to yaw, with the effective angle determined by calibration. The analog signals were filtered (low pass at 30 Khz), DC offset, and amplified ($\times 10$) before being fed into a computer interface. The interface contained a fast sample-and-hold A/D converter with 12-bit resolution and a multiplexer for connection to the computer. The wind tunnel reference pressure (used for normalizing the data) and temperature (used for correcting the cross-wire data) were also sampled by the computer. Individual velocity statistics were averaged over 5000 samples obtained at a rate of 400 samples per second – note that this relatively low sampling rate does not affect the time-

Streamwise location X (cm)	Streamwise location X/θ_0	Spanwise range Z/δ	Grid spacing (cm)	Grid size $Y \times Z$	Number of points per plane
8	68	45	0.10	21 × 91	1911
17	146	52	0.20	13 × 81	1053
37	325	14	0.25	21 × 61	1281
57	503	18	0.50	21 × 61	1281
78	681	14	0.50	25 × 61	1525
108	948	10	0.50	25 × 61	1525
128	1130	8	0.50	29 × 53	1537
189	1660	7	1.00	19 × 33	627
250	2200	5	1.00	23 × 31	713

TABLE 2. Data locations

averaged data presented exclusively in this article. The sampling time of 12.5 s corresponds to the passage of approximately 8500 spanwise vortices at the first measurement station – sensitivity studies have shown this to be an adequate sampling time for resolving both mean velocities and turbulence statistics.

Data were obtained in two planes (*uv* and *uw*) by rotating the cross-wire probe about its own axis. This method yielded all three components of mean velocity, five independent components of the Reynolds stress tensor and selected higher-order products. Extensive measurements were made at nine streamwise stations within the test section. Details of the measurement grids at the nine locations are given in table 2. The streamwise locations are normalized by the estimated initial mixing-layer momentum thickness: $\theta_0 = \theta_1 + \theta_2 = 0.114$ cm, and the spanwise extent of the measurement regions are normalized by the local mixing layer thickness, δ.

An error analysis, based on calibration accuracy and repeatability of measurements, indicates that mean streamwise velocity measurements with the cross-wire are accurate to within 3%, while mean cross-stream velocities are accurate to within 10%. Reynolds normal stress measurements are accurate to within 6%, and shear stresses are accurate to within 15–20%.

Spanwise velocity measurements in a mixing layer using a cross-wire probe are susceptible to contamination from the streamwise velocity gradient, which, owing to the orientation of the probe, is sensed as a contribution to the spanwise velocity. Accordingly, measurements of the spanwise mean velocity (W), and secondary shear stress ($\overline{u'w'}$), were corrected for the effects of the mean streamwise velocity gradient ($\partial U/\partial Y$), assuming a linear variation in quantities between the cross-wire sensors – details of the correction scheme are given in Bell & Mehta (1989*a*). The streamwise component of mean vorticity ($\Omega_x = \partial W/\partial Y - \partial V/\partial Z$) was computed using the central difference approximation to evaluate the derivatives of the secondary velocities. The mean streamwise vorticity measurements were repeatable to within about 20%. The overall circulation (Γ) was determined from the surface integral of the streamwise vorticity field over the cross-flow plane, with vorticity levels less than 20% of the maximum value being set to zero in order to provide immunity from 'noise'. Vorticity and circulation levels are presented throughout this paper in partially normalized form (divided by the velocity difference only), since the question of an appropriate lengthscale for the secondary vortex structure is still open. Therefore, the vorticity values given in this paper typically have units of cm^{-1} and the circulation values have units of cm.

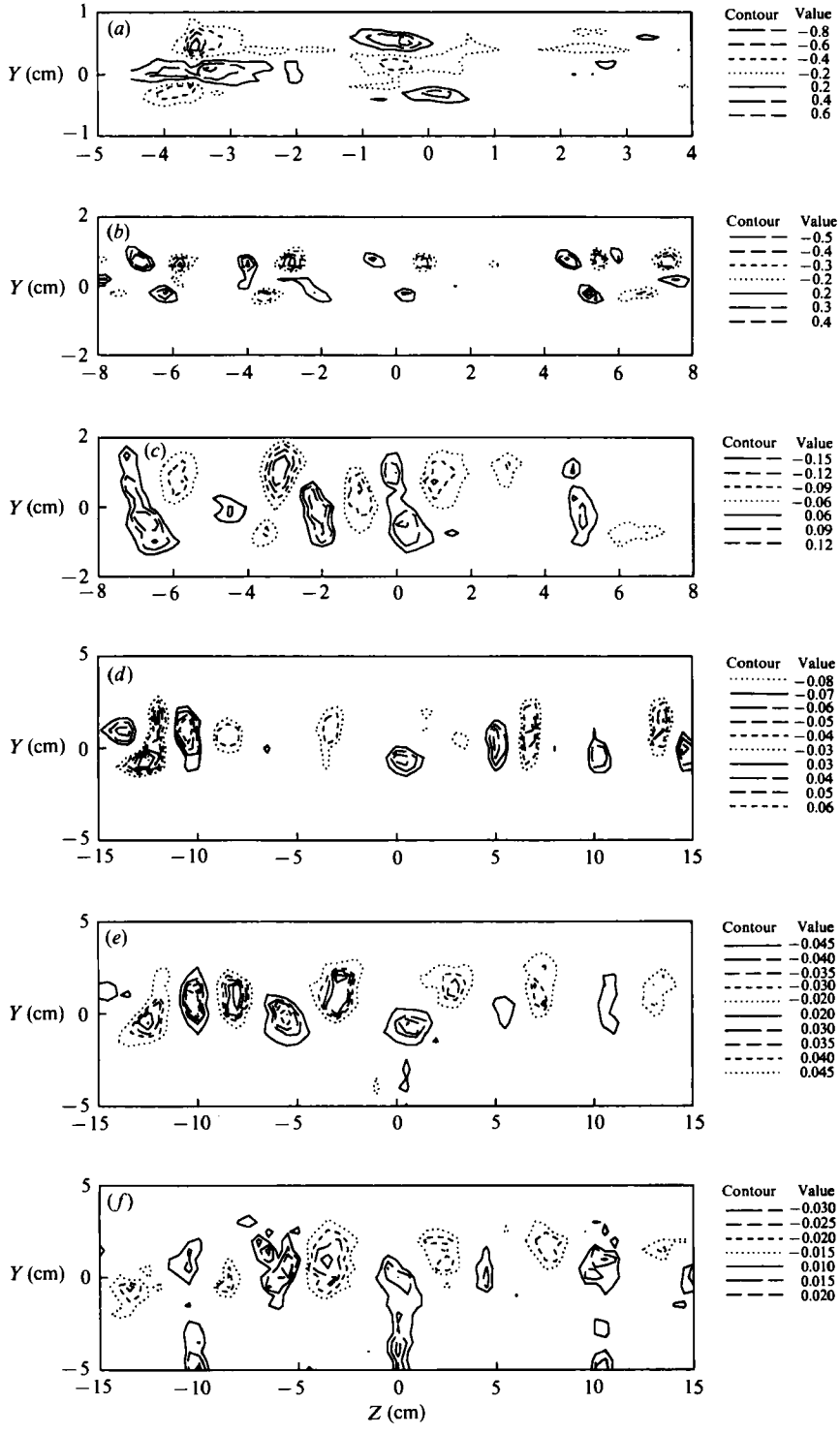

FIGURE 2(*a–f*). For caption see facing page.

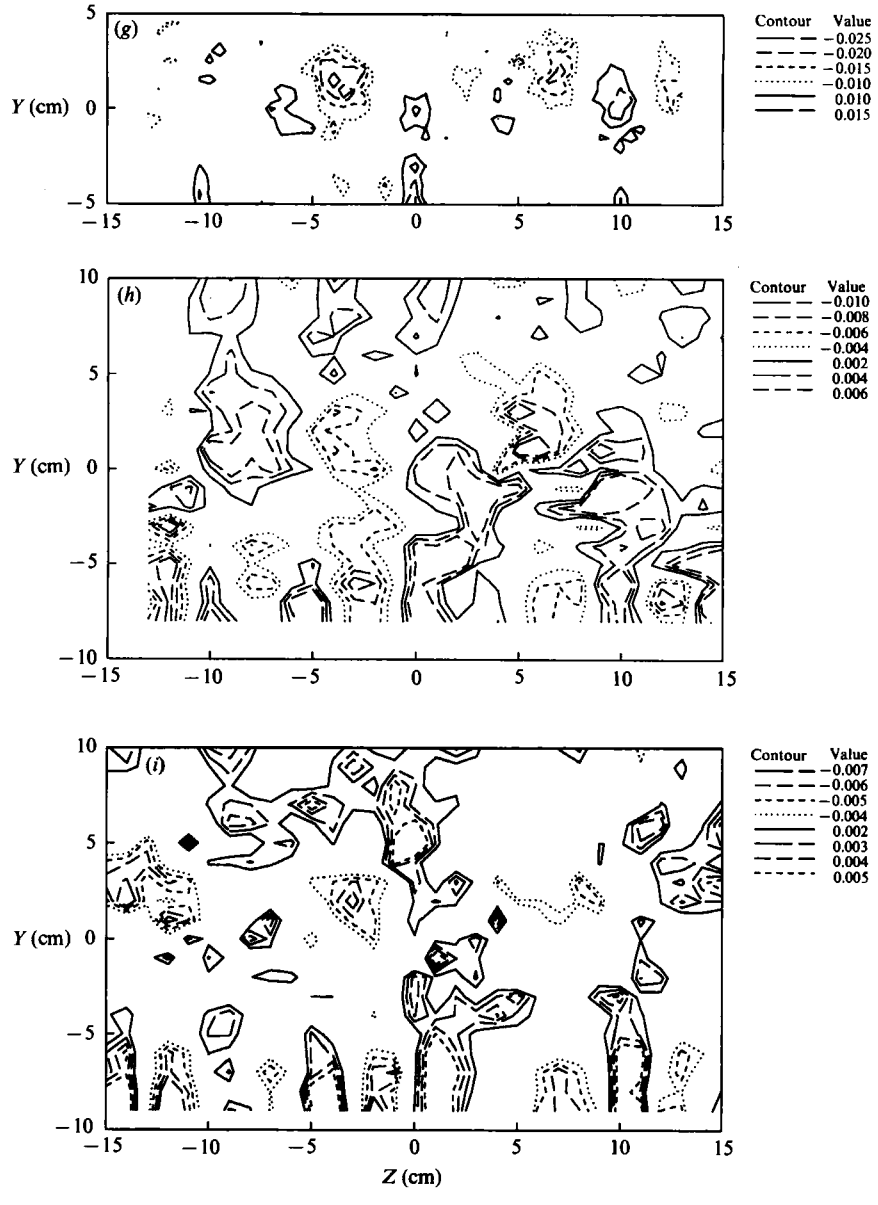

FIGURE 2. Mean streamwise vorticity (Ω_x/U_0, cm^{-1}) contours: (*a*) $X = 8$ cm; (*b*) 17 cm; (*c*) 37 cm; (*d*) 57 cm; (*e*) 78 cm: (*f*) 108 cm; (*g*) 128 cm; (*h*) 189 cm; (*i*) 250 cm.

3. Results and preliminary discussion

Three definitions for the mixing layer thickness were used in the present study. The conventional thickness, b, is defined as

$$b = (Y_{0.9} - Y_{0.1}), \tag{1}$$

where $Y_{0.9}$ and $Y_{0.1}$ are the cross-stream coordinates at which

$$U^* = (U - U_1)/(U_1 - U_2) = 0.9 \text{ and } 0.1,$$

respectively.

The mixing-layer vorticity thickness, δ_ω, is defined by the relation

$$\delta_\omega = \frac{U_1 - U_2}{(\partial U/\partial Y)_{\max}}. \tag{2}$$

The mixing-layer thickness can also be defined by fitting the mean streamwise velocity data to an expected profile shape. Following Townsend (1976), a mixing-layer thickness, δ, is defined using a fit of the velocity data to the error function profile shape:

$$U^* = \tfrac{1}{2}[1 + \mathrm{erf}(\zeta)], \tag{3}$$

where U^* is defined above, and ζ is the normalized y-coordinate:

$$\zeta = (Y - Y_0)/\delta. \tag{4}$$

The values of δ and Y_0 are determined by optimizing the error function fit.

3.1. *Mean streamwise vorticity*

Contour plots of mean streamwise vorticity, which only reflect the time-averaged behaviour of the flow field, are presented for the nine measurement stations in figure 2(*a–i*). Note that the vorticity scale is different for each station, since the peak levels drop rapidly with streamwise distance. At the first station ($X = 8$ cm), two relatively strong and organized 'clusters' of three streamwise vortices each are observed. Each cluster is made up of a central region of vorticity, which is elongated in the spanwise direction, and flanked by two vortices of opposite sign and lower aspect ratio. The signs of the central regions and their flanking vortices are reversed between the two clusters, which are approximately 3 cm apart. The clusters span the entire mixing-layer width, with the flanking vortices extending significantly beyond the $Y_{0.1}$ and $Y_{0.9}$ lines – this is further discussed in §§4.1.2 and 4.2.1.

A greater spanwise extent was covered at the second station ($X = 17$ cm), allowing a larger number of streamwise vortices to be measured. The most obvious change is that the vortices at this station are much rounder than those at the previous station. They are still found in clusters; approximately 17 vortices are seen here in four clusters. The average distance between the clusters is again about 3 cm. The two centre clusters appear to be continuations of those at $X = 8$ cm with the central region of vorticity split to form two vortices.

However, individual streamwise vortices cannot be reliably traced to the $X = 37$ cm station. Here a single row of about 12 vortices has begun to form. Peak vorticity varies widely from one vortex to the next, and vortices of the same sign can be found adjacent to one another, indicating that the realignment of the structures is still in progress. The double-peaked vortex near the centreline suggests that realignment is occurring, at least partly, through the amalgamation of adjacent vortices of the same sign.

By the $X = 57$ cm station, the streamwise vorticity has reorganized into a single row of alternating-sign vortices. Only about 11 vortices are measured at this station, across a span twice as wide as that of the previous station, thus indicating that the number of vortices per unit spanwise distance has been halved. Individual vortices can be easily traced between the $X = 57$ cm station and the next at $X = 78$ cm. The number of visible vortices remains the same, although the peak vorticity levels have decreased, and peak vorticity still varies considerably across the span from one vortex to the next. The unequal spacing observed between vortex pairs by Lasheras *et al.* (1986) is not apparent here, although it is possible that this asymmetry is

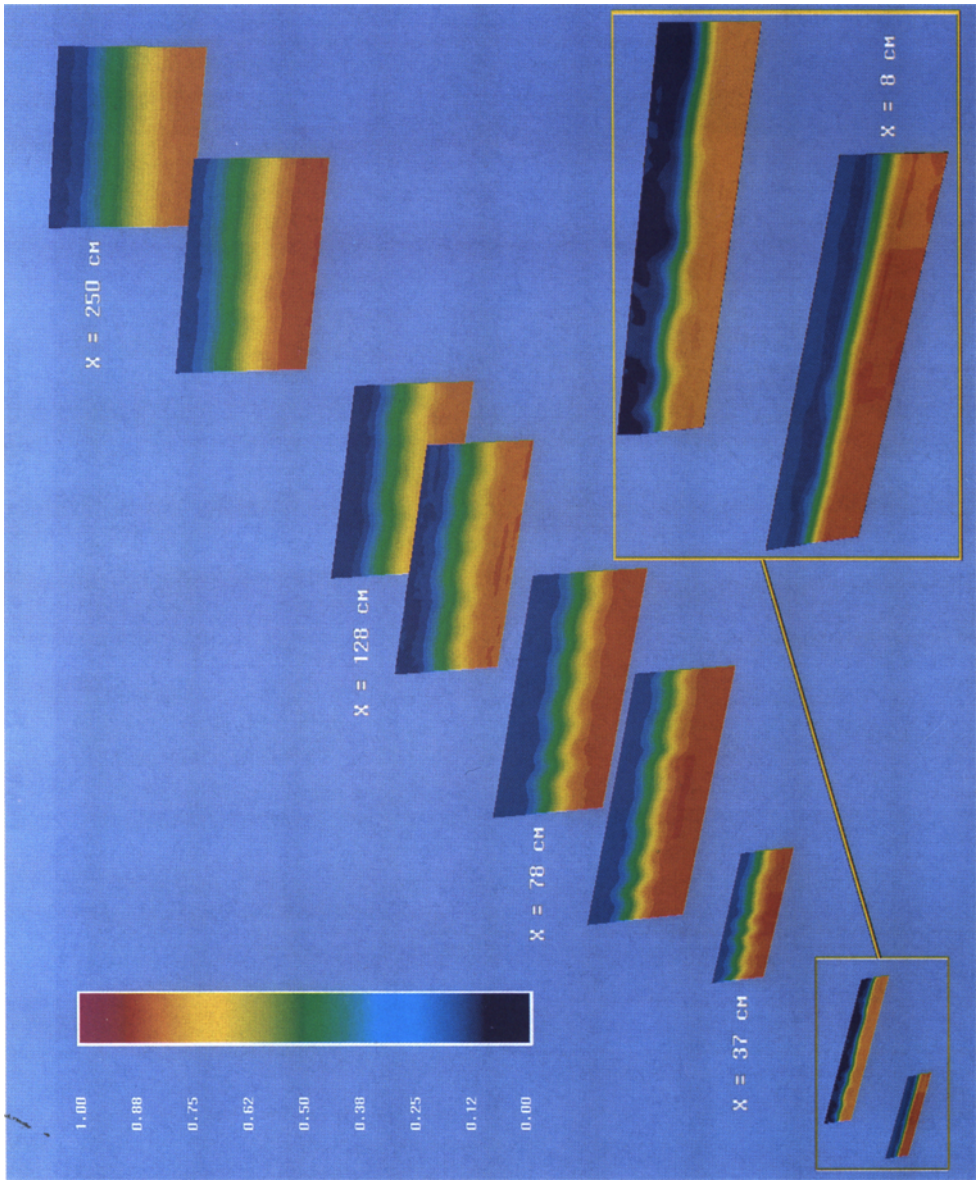

FIGURE 3. Mean streamwise velocity $((U - U_2)/U_0)$ contours.

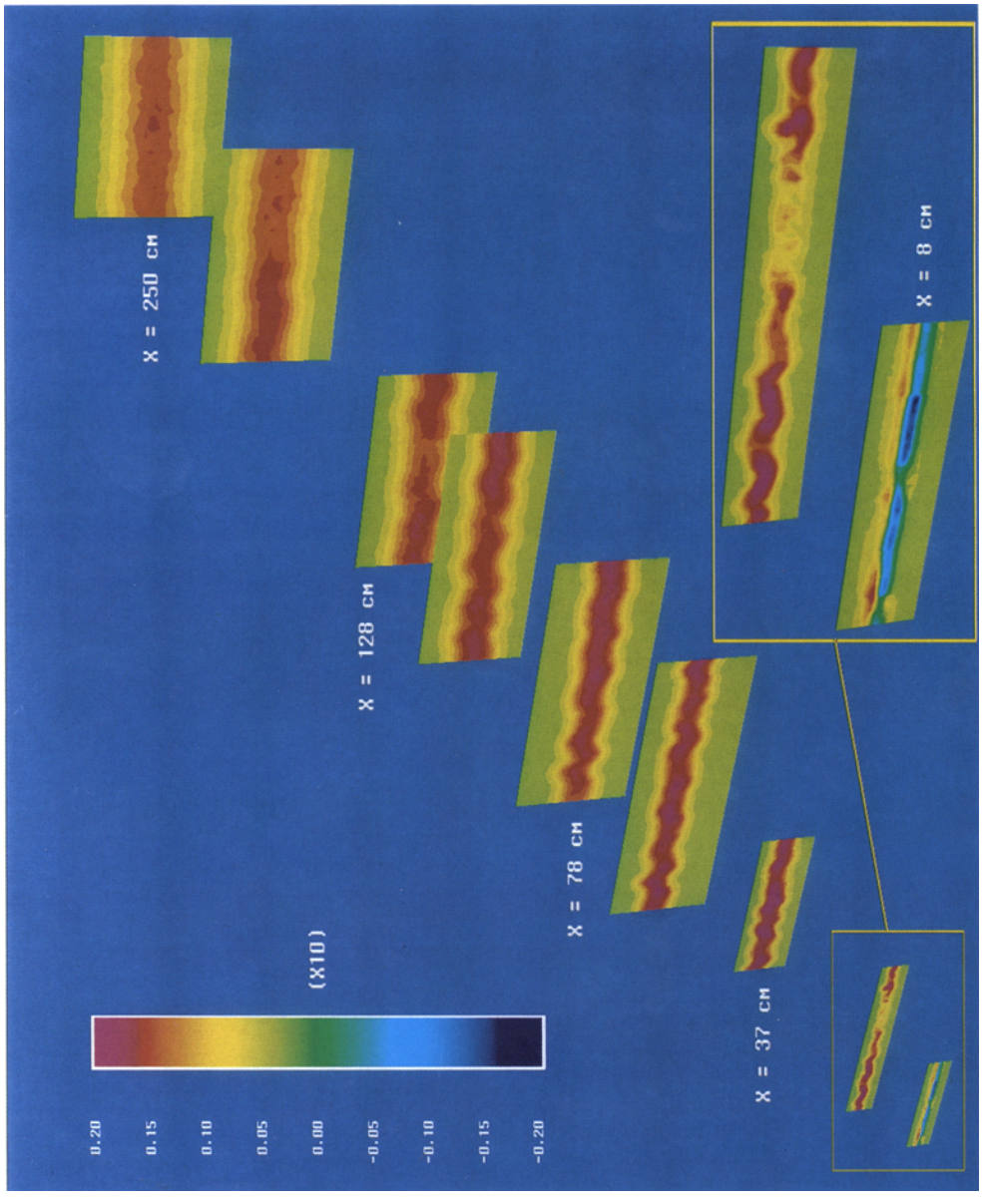

FIGURE 7. Primary shear stress ($\overline{u'v'}/U_0^2$) contours.

'averaged-out' in the present measurements. However, a slight asymmetry in position is apparent whereby the negative vortices are biased towards the positive-Y side – the reason for this apparent bias is not clear at this time.

By $X = 108$ cm, the vorticity contours are starting to acquire a slightly 'ragged' appearance, since the levels are decreasing relative to the 'noise'. However, the pattern of a single row of alternating-sign vortices is unchanged from the previous stations, as is the mean spanwise spacing of the vortices. This changes at $X = 128$ cm, where the number of discernable streamwise vortices drops to about six. At the $X = 189$ cm station, the streamwise vortices are virtually lost in the noise. However, a careful examination of the contour plot suggests that about five alternating-sign streamwise vortices can be found at this point in the mixing layer, indicating perhaps another increase in vortex spacing. By the last station ($X = 250$ cm), the low level of organized streamwise vorticity becomes indistinguishable from the background noise level.

The general trends of the vorticity data include reorganization from a complex initial pattern, consisting of clusters of vortices, to a single row of alternating-sign vortices, accompanied by an increase in vortex size and spacing and a decrease in peak mean vorticity levels.

3.2. *Mean streamwise velocity and Reynolds stresses*

The presence of concentrated streamwise vorticity is found to significantly affect the distribution of mean velocity and Reynolds stresses within the mixing layer. Contours of the mean streamwise velocity are presented in figure 3 (plate 1). Initially, at the $X = 8$ cm station, only a few isolated 'kinks' are seen in the streamwise velocity contours. These increase in number and become stronger by $X = 17$ cm. Downstream of $X = 17$ cm, the spanwise variation in the mean streamwise velocity mostly takes the form of a wrinkling of the mixing layer, with apparently little change in thickness. The wrinkling first appears at irregular intervals, becomes more regular at about the $X = 78$ cm station, and retains this character, albeit with decreasing amplitude and increasing wavelength, as the flow evolves downstream. By the last measurement station at $X = 250$ cm, the contours appear more or less straight and parallel, implying that the mixing layer is nominally two-dimensional. The wrinkling is a result of the cross-stream transfer of axial momentum by the streamwise vortices, such that a peak in the mean streamwise velocity contours is generated by a vortex pair with common flow upwards and vice versa. The amplification and subsequent decay of the wrinkling is seen more clearly in figure 4, where the spanwise variation in velocity along the nominal mixing-layer centreline is plotted for each streamwise location. The maximum peak-to-peak amplitude of the variation is approximately 10%. In contrast, the variations measured by Jimenez (1983) and Huang & Ho (1990) were higher (40% and 20%, respectively), whereas those of Wood (1982) were about the same as the present case and those of Plesniak & Johnston (1989) somewhat lower (5%). The fact that such variations have been measured in different facilities using different techniques suggests that the appearance of the streamwise vorticity is more likely a result of an instability mechanism, rather than an artifact of the facility design or its flow quality. However, the relatively large scatter in the measured peak-to-peak amplitudes does imply that the strengths of the generated vortices may be facility dependent, especially since there seems to be no obvious correlation between them and the operating conditions, such as velocity ratio or Reynolds number.

In order to investigate the quantitative nature of the wrinkling in the mixing

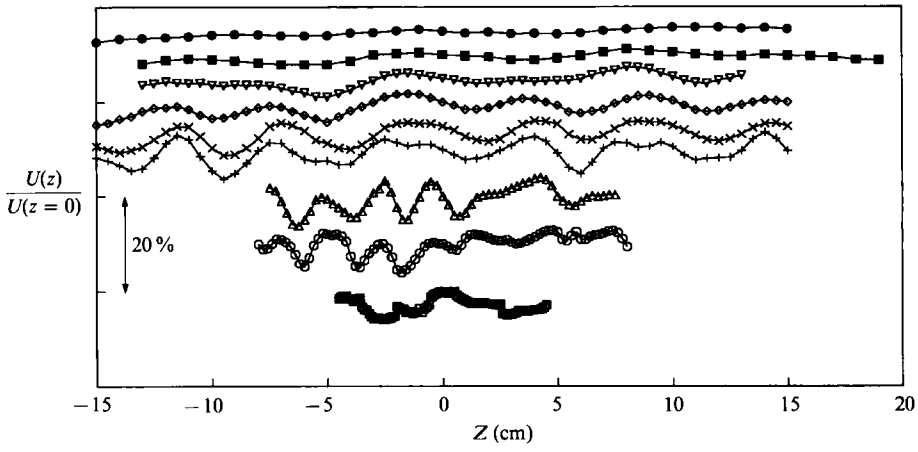

FIGURE 4. Spanwise variation of mean velocity (U) along $Y = 0$ at nine streamwise stations: □, $X = 8$ cm; ○, 17 cm; △, 37 cm; +, 57 cm; ×, 78 cm; ◇, 108 cm; ▽, 128 cm; ■, 189 cm; ●, 250 cm.

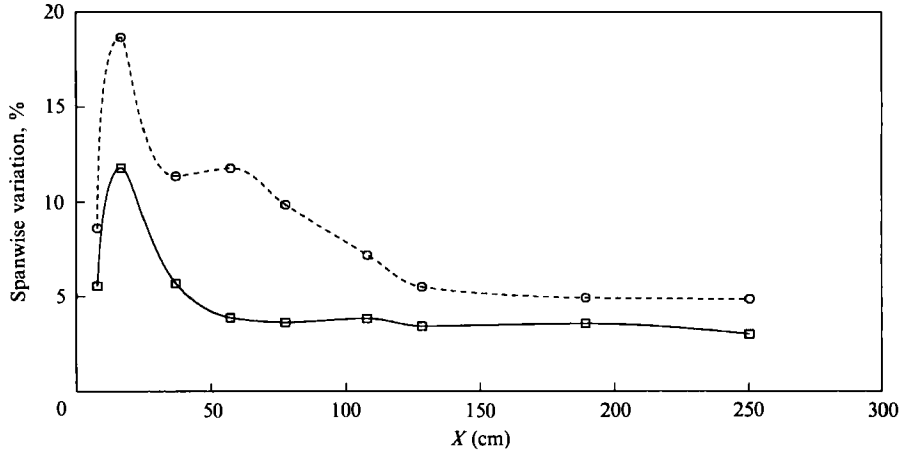

FIGURE 5. Streamwise development of spanwise variation in mixing-layer thickness and distortion: □, standard deviation of δ; ○, standard deviation of Y_0/δ.

layer, the standard deviation of the layer thickness (δ) and centreline location (Y_0) are plotted as a function of X in figure 5. The standard deviation of δ is an indicator of the spanwise variation in mixing-layer thickness, while the standard deviation of Y_0 indicates how much bending or distortion is present in the layer. Initially, the scatter in both quantities is relatively low, but increases markedly at the $X = 17$ cm station. Beyond this location, the variation in δ quickly drops to a low level, as does that of Y_0, although at a lower rate. In the region $X = 40$–130 cm, the variation of Y_0 is much higher than that of δ, indicating that the mixing layer is wrinkled bodily in the spanwise direction, without much variation in thickness. Both the mixing-layer centreline and thickness show relatively small variations beyond $X \sim 130$ cm, implying that the mixing layer has recovered to a more or less two-dimensional state.

The presence of streamwise vorticity also produces significant spanwise variations in the three Reynolds normal stresses ($\overline{u'^2}$, $\overline{v'^2}$ and $\overline{w'^2}$). The distribution of the normal stresses at the first station ($X = 8$ cm) is shown in figure 6(a–c), which serves to

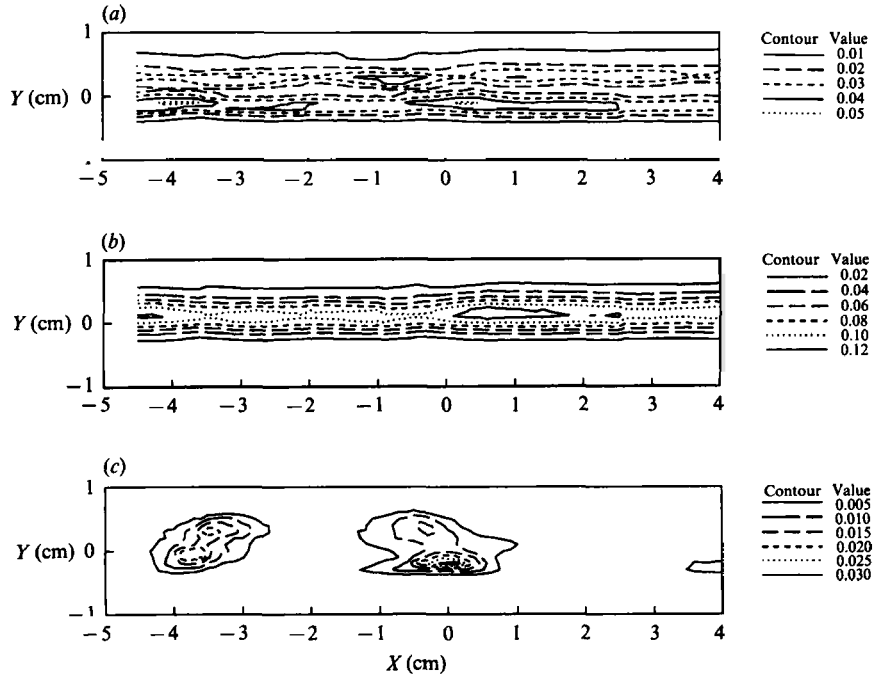

FIGURE 6. Normal-stress contours at $X = 8$ cm. (*a*) $\overline{u'^2}/U_0^2$; (*b*) $\overline{v'^2}/U_0^2$; (*c*) $\overline{w'^2}/U_0^2$.

illustrate the three-dimensional nature of the turbulence field at this point. The $\overline{u'^2}$ distribution (figure 6*a*) consists of two 'ridges' of high $\overline{u'^2}$, separated by a relatively low 'trough'. This behaviour most likely reflects the dominance of the near-field turbulence by the orderly passage of well-organized spanwise vortices. The central region of each vortex is relatively quiescent, with higher u-fluctuations around the periphery, which results in the characteristic 'double-ridge' distribution of $\overline{u'^2}$. Several local peaks of $\overline{u'^2}$ can be discerned in the figure, the strongest of which occur at the same location as the streamwise vortices. As noted previously (Bell & Mehta 1990*a*), a streamwise vortex embedded in a mixing layer will generally enhance normal stress levels at its location since the vortex-generated cross-flows and distortions produce additional mean velocity gradients, resulting in increased turbulence production. Figure 6(*b*) shows that the $\overline{v'^2}$ distribution, in contrast, is dominated by very high levels along the mixing-layer centreline. Again, this is presumably due to the initial roll-up and organized passage of the spanwise vortices in the near-field region, since each vortex produces a strong vertical perturbation. Local peaks are also seen in the $\overline{v'^2}$ distribution, and these are again roughly coincident with the location of the vortex clusters, but their levels are about 2.5 times higher than the peak $\overline{u'^2}$ levels. Lastly, figure 6(*c*) shows that the initial distribution of $\overline{w'^2}$ is entirely dominated by isolated peaks, which are also roughly coincident with the streamwise vortex clusters and carry peak levels equivalent to about 60 % of peak $\overline{u'^2}$. It appears that initially almost all the $\overline{w'^2}$ in the mixing layer is generated through the interaction of the streamwise vortices with the mixing layer. This is not too surprising since, initially, the organized spanwise vortices would not be expected to contribute much to $\overline{w'^2}$. Further downstream, as the coherence of the spanwise structures decays and the mixing layer becomes turbulent, the distributions of the normal stresses evolve into a single 'ridge' extending in the spanwise direction.

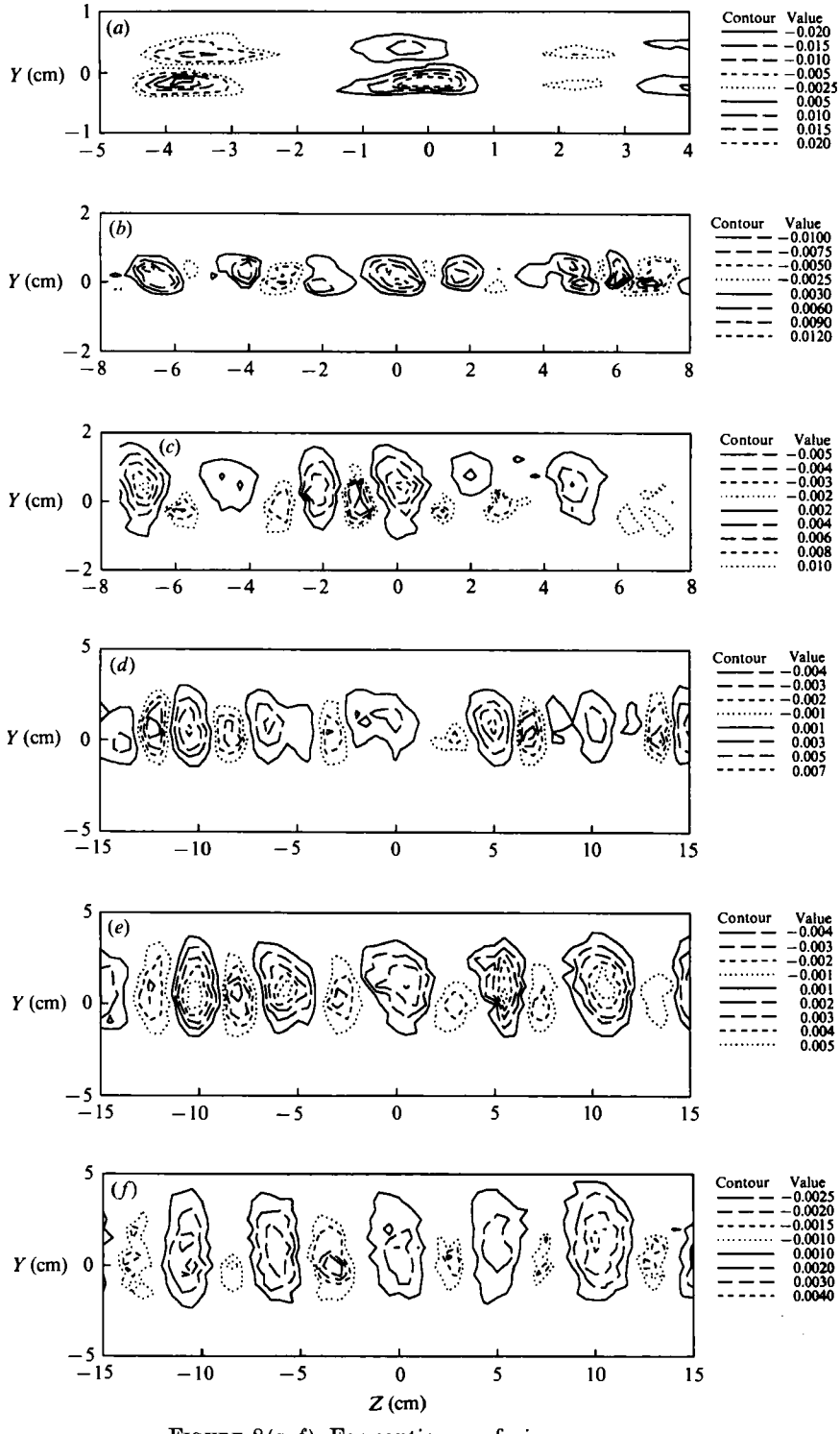

FIGURE 8(*a–f*). For caption see facing page.

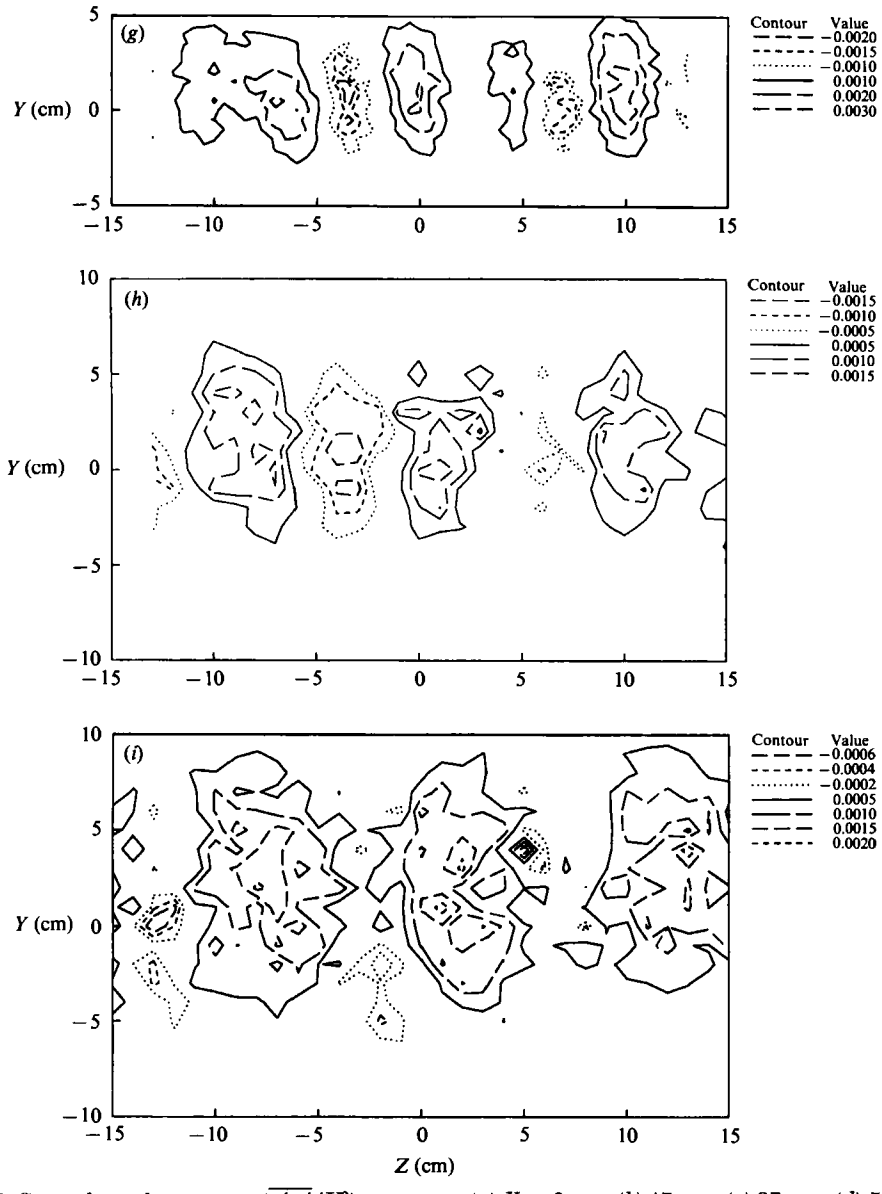

FIGURE 8. Secondary shear stress ($\overline{u'w'}/U_0^2$) contours: (*a*) $X = 8$ cm; (*b*) 17 cm; (*c*) 37 cm; (*d*) 57 cm; (*e*) 78 cm; (*f*) 108 cm; (*g*) 128 cm; (*h*) 189 cm; (*i*) 250 cm.

The spanwise variations also decrease further downstream such that an essentially two-dimensional distribution of normal stresses is observed at the last measurement station ($X = 250$ cm).

Large spanwise variations are also observed in the primary shear stress ($\overline{u'v'}$) distributions (figure 7, plate 2). At the first station ($X = 8$ cm), $\overline{u'v'}$ is almost entirely negative, as a result of the organized passage of the spanwise vortices alluded to previously. It is interesting to note that positive $\overline{u'v'}$ is generated at the positions of the vortex clusters, decreasing the magnitude of negative $\overline{u'v'}$ at these locations. As a result, the spanwise variation of $\overline{u'v'}$ at this station is as large as the cross-stream variation. At the second station, positive $\overline{u'v'}$ is being generated throughout the

mixing layer, but the $\overline{u'v'}$ distribution is still dominated by local peaks, which results in order-of-magnitude variations in $\overline{u'v'}$ along the centreline. There is no obvious correlation between the distribution of $\overline{u'v'}$ and the streamwise vortices, although the contours do exhibit the characteristic wrinkling at this station. The expected correlation was that noted in the previous study of a streamwise vortex embedded in a mixing layer (Bell & Mehta 1990*a*), where it was found that a dip in $\overline{u'v'}$ was generated at the vortex position with a peak on either side. With several vortices embedded in the mixing layer, not always in a regular array, it is quite possible that the distribution of $\overline{u'v'}$ would end up being too complex to interpret easily. Downstream of the first two stations, the distribution of $\overline{u'v'}$ takes on the same pattern of local peaks and wrinkles as the normal stresses, but with more spanwise variation. In the far-field region, the variation in $\overline{u'v'}$ also decreases and by $X = 250$ cm, the distribution appears nominally two-dimensional.

The secondary shear stress ($\overline{u'w'}$) contours for the nine measurement stations are shown in figure 8(*a–i*). Note that the measured $\overline{u'w'}$ would normally be negligible compared to $\overline{u'v'}$ in a two-dimensional mixing layer. In the present mixing layer, however, relatively large levels of positive and negative $\overline{u'w'}$ are observed in the form of individual peaks. Initially, the peaks are irregularly distributed, but downstream of $X = 37$ cm, they become aligned into a single row of alternating-sign peaks, in a manner similar to the evolution of the streamwise vorticity contours. A direct comparison between the $\overline{u'w'}$ and the streamwise vorticity contours reveals several interesting points.

At the first station ($X = 8$ cm), peaks in $\overline{u'w'}$ appear at the location of the spaces between the streamwise vortices, where the strongest cross-flow gradients are generated, but no obvious correlation is observed at the second station ($X = 17$ cm). Streamwise vorticity appears in clusters, while the $\overline{u'w'}$ distribution takes the form of a single row of peaks of alternating sign, with two exceptions where peaks of like sign occur adjacent to one another. The levels of positive and negative $\overline{u'w'}$ are not symmetrically distributed at this station; the peak level of positive $\overline{u'w'}$ is about 30% greater than the peak absolute level of negative $\overline{u'w'}$. At the third station ($X = 37$ cm), the correspondence between the distributions of streamwise vorticity and $\overline{u'w'}$ is remarkably good. With one exception, each peak in $\overline{u'w'}$ appears at the same location as the peak in Ω_x, with signs consistent. At one point, a peak in $\overline{u'w'}$ appears where a streamwise vortex would be expected to maintain the alternating-sign pattern. The one-to-one correlation between Ω_x and $\overline{u'w'}$ is also observed at all the downstream stations; scale and spacing changes in Ω_x are mirrored by similar changes in the $\overline{u'w'}$ distribution, all the way up to the last station ($X = 250$ cm). Although the levels of $\overline{u'w'}$ are very low at this last station, a pattern of alternating-sign peaks can still be discerned, with the positive $\overline{u'w'}$ levels about three times as high as the negative levels. The reason for this asymmetry in the levels is not clear at this point, although further investigations on this phenomenon are underway. As with the peak streamwise vorticity, the peak levels of both positive and negative $\overline{u'w'}$ decrease monotonically with streamwise distance.

3.3. *Self-similarity of the mixing layer*

Townsend (1956) showed that, for sufficiently high Reynolds number and downstream distance, the governing equations and boundary conditions for the plane turbulent mixing layer can yield 'self-similar' solutions. The distinguishing features of a self-similar mixing layer are that the layer grows linearly and that the shapes of the mean velocity and turbulence profiles are independent of downstream

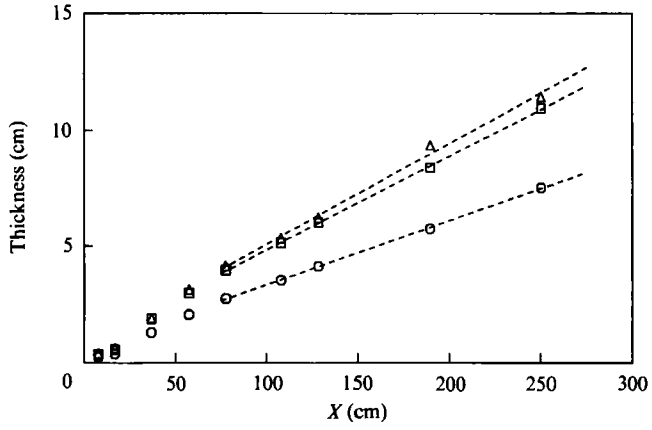

FIGURE 9. Streamwise development of mixing-layer thickness: □, $b = Y_{0.9}-Y_{0.1}$; ○, δ; △, δ_ω.

db/dx	$d\delta_\omega/dx$	$d\delta/dx$	X_0 (cm)	X_D (cm)
0.042	0.044	0.023	−18	75

TABLE 3. Mixing-layer growth parameters

distance when scaled by local velocity and length scales – these are generally represented by the velocity difference across the mixing layer and its width. A self-similar mixing layer with universal behaviour which is completely independent of initial conditions is, however, hardly ever realized in practice (Rodi 1975). The main reason for this discrepancy is the fact that mixing layers are inherently very sensitive to initial and operating conditions, the effects of which often persist for relatively long distances downstream of the origin (Birch 1981; Mehta & Westphal 1986; Mehta 1991). The issue of self-similarity may be complicated even more by the present revelations regarding the three-dimensional structure of plane mixing layers.

3.3.1. *The behaviour of the mixing-layer growth rates*

Since large spanwise variations are experienced in the near-field distribution of the streamwise velocity, an averaging scheme has been employed in the present study so as to obtain an accurate representation of the overall behaviour of the mixing layer. The measured plane of data is split into individual profiles across the layer and the mixing-layer thickness is computed for each profile separately. The evaluated thickness is then averaged over all the spanwise positions in the mixing layer. All the values of b, δ_ω, and δ presented below were spanwise averaged using this approach. The mixing-layer growth rates, using all three definitions for layer thickness, are presented in figure 9 and table 3. X_D is the development distance beyond which all three measures of mixing-layer thickness increase linearly with streamwise distance, and X_0 is the average virtual origin extrapolated from the three measures of mixing-layer thickness.

Previous studies have shown a dependence of the different measures of the growth rate on the free-stream velocity ratio (Rodi 1975). The effect of velocity ratio on growth rate has been determined analytically by Abramovich (1963) and Sabin (1965) giving the relation

$$\sigma_0/\sigma = \lambda = (1-r)/(1+r), \tag{5}$$

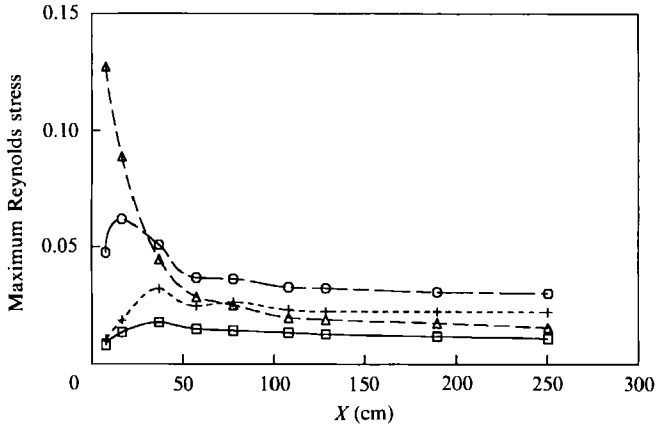

FIGURE 10. Streamwise development of maximum Reynolds stresses: □, $\overline{u'v'_{max}}/U_0^2$; ○, $\overline{u'^2_{max}}/U_0^2$; △, $\overline{v'^2_{max}}/U_0^2$; +, $\overline{w'^2_{max}}/U_0^2$.

where σ is the spreading parameter [$= 1/(\mathrm{d}\delta/\mathrm{d}X)$], and σ_0 is the spreading parameter for a single-stream mixing layer. Using the commonly accepted value of 11 for σ_0 gives a predicted growth rate, $(\mathrm{d}\delta/\mathrm{d}X) = 0.023$, the same as the measured value. Brown & Roshko (1974), following Liepmann & Lauffer (1947), suggest that the best fit to the vorticity-thickness spreading rate data is given by

$$\mathrm{d}\delta_\omega/\mathrm{d}x = 0.16\lambda. \tag{6}$$

For the present case, $\lambda = 0.25$, resulting in an expected value of $\mathrm{d}\delta_\omega/\mathrm{d}x = 0.040$ – only about 10% lower than the measured value. So, as far as the growth of the present mixing layer is concerned, it seems to follow the expected behaviour and does not represent a 'pathological' case.

3.3.2. *Behaviour of the peak Reynolds stresses*

A more accurate indicator of mixing-layer development is the behaviour of the peak Reynolds stresses. By definition, if a two-dimensional mixing layer is to approach a self-similar state, the maximum value of all components of the Reynolds stress tensor must asymptote to a constant level. Typically, this is taken to refer to the behaviour of the normal stresses ($\overline{u'^2}$, $\overline{v'^2}$ and $\overline{w'^2}$) and the primary shear stress ($\overline{u'v'}$). The behaviour of the maximum Reynolds stresses before reaching the asymptotic limit is found to depend on the initial conditions of the mixing layer (Bradshaw 1966; Mehta & Westphal 1986). The maximum measured Reynolds stresses are plotted against streamwise distance in figure 10. The maximum stresses are also spanwise averaged – the maximum stress for each profile is located individually and then averaged over all the spanwise locations. The Reynolds stresses follow the expected 'overshoot' pattern for approach to self-similarity in a mixing layer originating from laminar initial conditions. The overshoot is most marked in $\overline{v'^2_{max}}$, which peaks at over seven times its asymptotic level, while $\overline{u'^2_{max}}$ and $\overline{w'^2_{max}}$ peak at twice and 1.5 times their asymptotic levels, respectively. Also, $\overline{v'^2_{max}}$ peaks first, at around $X = 8$ cm, with $\overline{u'^2_{max}}$ peaking at $X \sim 17$ cm, followed by $\overline{w'^2_{max}}$ at $X \sim 37$ cm. These results imply that a part of the overshoot, especially that in $\overline{v'^2_{max}}$, is a result of the initial roll-up of the spanwise structures. Energy is then transferred into the streamwise and spanwise fluctuations further downstream. Downstream of $X = 100$ cm, the stresses appear to achieve more or less constant

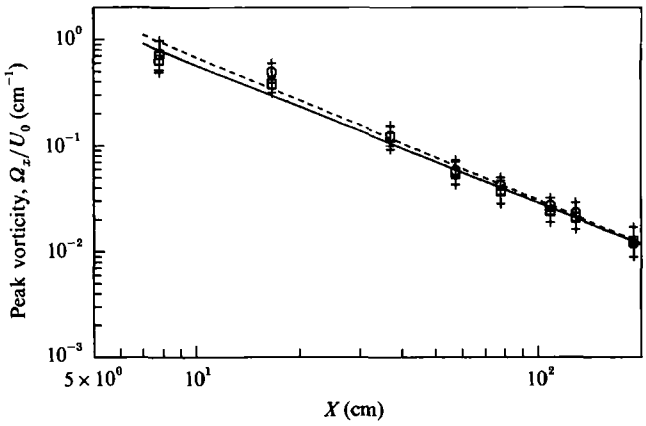

FIGURE 11. Streamwise development of peak mean streamwise vorticity; error bars represent standard deviation of spanwise variation: □, positive vorticity; ○, ABS (negative vorticity); ——, best fit to positive data (equation (7*a*)); – – – –, best fit to negative data (equation (7*b*)).

$\overline{u'^2_{\max}}$	$\overline{v'^2_{\max}}$	$\overline{w'^2_{\max}}$	$\overline{q^2_{\max}}$	$\overline{u'v'_{\max}}$
0.0306	0.0165	0.0224	0.0695	0.0114

TABLE 4. Maximum measured Reynolds stresses

levels, which may normally be taken as the distance at which a self-similar state is reached. The measured values of the maximum Reynolds stresses at the last station are given in table 4.

The peak level of $\overline{q^2_{\max}}$ agrees reasonably well with the average results given by Rodi (1975) for two-stream mixing layers of comparable velocity ratio. One interesting point brought out by the tabulation of maximum Reynolds stresses is that $\overline{u'v'_{\max}}$ asymptotes to approximately 0.011 which is exactly the value computed by Townsend (1976) for a self-similar plane mixing layer using Sabin's (1965) value for the entrainment parameter. The question of self-similarity of the present mixing layer is further discussed below in §4.3.1.

4. Further discussion

4.1. *Overall properties of the streamwise vorticity*

4.1.1. *Mean streamwise vortex strength*

At a given streamwise location, the magnitudes of peak mean vorticity and circulation vary significantly from one vortex to the next. The standard deviation of the peak vorticity levels is generally about 25% of the mean value. The variation in circulation is even greater; the standard deviation being typically about 50% of the mean value. There is no discernible pattern to the variations in peak vorticity and circulation levels at each station. Consequently, only the spanwise-averaged results are presented here, although positive and negative vortices are averaged separately, in order to detect any global differences in their behaviour.

The average value of peak vorticity at each station is plotted on a log–log scale, for both positive and negative vorticity, in figure 11. The 'error bars' accompanying each data point represent the standard deviation of the spanwise variation of the

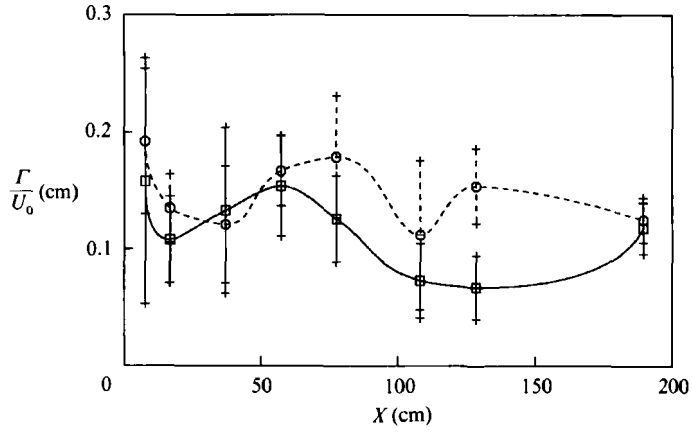

FIGURE 12. Streamwise development of average streamwise vortex circulation; error bars represent standard deviation of spanwise variation: □, positive circulation; ○, ABS (negative circulation).

values. The peak streamwise vorticity at the first station is equivalent to about 30% of the peak spanwise vorticity, which is in agreement with the estimates of Huang & Ho (1990), based on their measurements of 'partial streamwise vorticity' ($\partial V/\partial Z$). The peak vorticity drops monotonically, with both the positive and negative values following approximately the same decay curves. The average peak negative level is initially about 15% higher than the positive level, but the negative vorticity appears to decay slightly faster and so beyond $X = 50$ cm downstream, the positive and negative levels agree to within 5%. The shape of the decay curves suggest a power-law-type decay of the form $\Omega_{x_{\max}} = A(X-X_0)^B$. The parameters A and B were estimated using a logarithmic least-squares fit to the data, with the error of the fit minimized by the choice of X_0, the 'virtual origin' of the vortices. This fitting procedure yielded the following relations:

positive mean vorticity decay rate

$$\Omega_{x_{\max}}/U_0 = 30(X+4.5)^{-1.50}; \tag{7a}$$

negative mean vorticity decay rate

$$\Omega_{x_{\max}}/U_0 = 51(X+5.5)^{-1.59}. \tag{7b}$$

These results confirm the initial impression that the negative vorticity decays slightly faster. However, since the difference in decay rates is only about 6%, it is concluded here that the overall mean streamwise vorticity decays as approximately $1/X^{1.5}$.

The average streamwise circulation (figure 12) remains relatively constant throughout the measurement region, with a temporary increase around $X = 50$–70 cm, in both the positive and negative levels. Once again, the 'error bars' show the large spanwise variation in strength between vortices at a given station. The estimates obtained by Jimenez (1983) also suggested that the streamwise vortex circulation was approximately constant. The measured initial circulation (average of all vortices) in the present study is $\Gamma/U_0 = 0.17$ cm, which corresponds to about 10% of the estimated spanwise circulation of the initial Kelvin–Helmholtz roll-up. This is the first time that the streamwise circulation has been measured directly, and it is interesting to note that the initial circulation level is significantly lower than the previous estimates; Jimenez (1983), Jimenez *et al.* (1985) and O'Hern (1990) all suggested that the initial streamwise vortex circulation was of the same order as that

of the initial spanwise roll-up. The difference in strength between the positive and negative vortices is clearly visible in this case, although the difference is less than the standard deviation of the measurements across the span.

It must be noted that these results reflect only the *mean* behaviour of the streamwise vortex structure. The present results cannot resolve the possibility of large-scale motion of the structure as a whole which is further discussed in §4.3.2.

4.1.2. *Spanwise disturbance wavelength and vortex spacing*

Streamwise vortices in mixing layers are found to occur in a quasi-periodic pattern, consisting of either a row of single vortices or, as seen in the very near field of the present study, clusters of vortices. The mean spacing between vortices (or clusters) can be determined directly from vorticity measurements, as done here, or inferred from flow visualization results (Breidenthal 1978; Lasheras *et al.* 1986). More indirect ways to measure the vortex spacing rely on the fact that the streamwise vortices produce spanwise variations in the mean velocities and Reynolds stresses (Jimenez 1983; Huang & Ho 1990). For example, a single row of alternating-sign streamwise vortices in a mixing layer generates upwash and downwash in between the vortices, thus producing wrinkles in the velocity contours. The wavelength associated with this variation, Λ, is simply twice the streamwise vortex spacing. However, streamwise velocity variations depend on the pattern and strengths of the streamwise vortices, as well as their spacing; a simple relationship between the two exists only when the vorticity distribution itself is sufficiently simple and regular. In the present study, the vortex spacing (s) and the spanwise disturbance wavelength (Λ) are determined as follows:

(i) The streamwise vortex spacing is evaluated by simply counting the number of streamwise vortices per unit span shown on the contour plots. A concentration of vorticity is considered to be a vortex if it includes at least two closed contours, arranged concentrically. The contour levels are, in turn, typically chosen such that this will include all vortices with peak levels equivalent to at least 40 % of the highest vorticity level measured at that station. This procedure ensures that vorticity contours resulting from noise will not be counted, the cost being the failure to count the really weak vortices. Vortices partially cut off at the ends of the measurement domain are counted as half of a vortex. Since each streamwise vortex appears to be associated with a peak in $\overline{u'w'}$, and since the $\overline{u'w'}$ contour plots often appear more regular than the Ω_x contour plots, the peaks in $\overline{u'w'}$ are counted for verification, using the same procedure as for the streamwise vorticity.

(ii) The spanwise disturbance wavelength, Λ, is determined by taking the Fourier transform of the isovelocity lines, $Y_{0.1}$, $Y_{0.5}$, and $Y_{0.9}$, and taking the peak wavelength visible in all three transforms. This procedure ensures that the disturbance whose wavelength is being counted extends across the entire mixing layer. In addition to the Fourier transform, the maximum entropy method (Andersen 1974), which is less sensitive to small data set size, was also used to obtain a second estimate of the wavelength. In the present case, both these techniques gave essentially the same estimate of the spanwise disturbance wavelength and so only the Fourier transform results are discussed below.

Each of these two methods has both merits and demerits. Vortex counting depends to some extent on the choice of contour levels, especially if the vortices themselves are not very well defined. The existence of merging and/or elongated vortices presents a difficulty, since it is not clear how to tell one from the other. On the other hand, Λ may not be an accurate indicator of the vortex structure spacing either. As

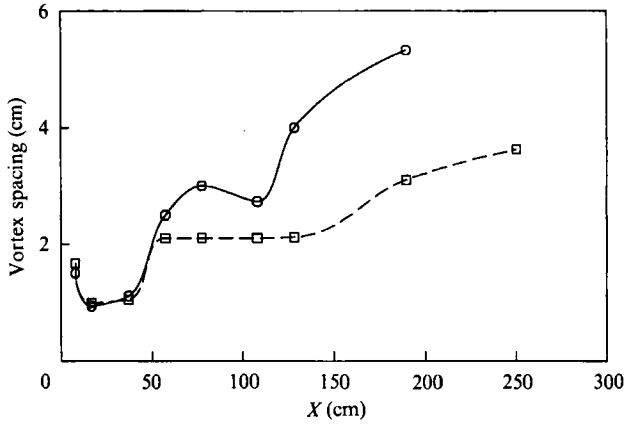

FIGURE 13. Streamwise development of vortex spacing and disturbance wavelength: □, ½(spanwise disturbance wavelength); ○, vortex spacing.

noted above, $\Lambda = 2s$ is strictly true only when the vortices are arranged in a single row, and thus Λ is an unreliable measure when there is significant clustering of vortices, as seen in the near field of the current experiment. The results of both techniques applied to the present data are shown in figure 13. Although some differences exist between the actual values given by the two techniques, the qualitative trends are the same. On the whole, we feel that direct vortex counting provides a more accurate estimate of the streamwise vortex structure spacing.

The average vortex spacing at the first station is determined by vortex counting to be 1.5 cm, which is 88% of the 1.7 cm Kelvin–Helmholtz wavelength associated with the spanwise vortices. However, the cluster spacing is approximately 3.3 cm, which is about twice the Kelvin–Helmholtz wavelength. Previous measurements from flow-visualization studies (Konrad 1976; Breidenthal 1978; Jimenez *et al.* 1985; Lasheras *et al.* 1986) have all indicated that the initial wavelength is approximately equal to the initial Kelvin–Helmholtz wavelength of the spanwise vortices.

The mean vortex spacing drops at the second station ($X = 17$ cm), to 0.94 cm, rather than growing with mixing-layer thickness. A similar phenomenon was inferred by Jimenez (1983) from his streamwise velocity measurements. Jimenez noted that the spanwise disturbance wavelength decreased with X upstream of $X = 100\theta_0$, a distance which corresponds to $X = 11$ cm in the present study (assuming $\theta_0 = \theta_1 + \theta_2$ for the two-stream layer). In the present study, this decrease can be attributed to the evolution of the vortex clusters seen at the first station. Comparing the streamwise vorticity distributions at the first two stations (figures 2*a* and 2*b*), it is seen that the clusters consist of three vortices at the first station and generally four at the second. The increase in the number of vortices per cluster appears to be a result of the central vortex splitting in two. If splitting of the central vortex is a common occurrence, it would increase the number of vortices per unit span by up to 30%, which would account for the difference noted between the first and second stations.

The vortex spacing increases by approximately a factor of two between the $X = 37$ cm and $X = 57$ cm stations. An examination of the vorticity contour plots at these locations (figures 2*c* and 2*d*) shows that the streamwise vortices are organized in a single row at both stations. Between these two stations, some process occurs which cuts the number of vortices per unit span in half while maintaining the single-row organization. The sudden jump in vortex spacing over a short distance suggests

that some form of vortex cancellation or amalgamation is taking place. A second jump is seen further downstream, at about $X = 120$ cm. This suggests that the same process can occur repeatedly as the flow evolves downstream, and that it is the mechanism by which the streamwise vortices periodically adjust themselves to the mixing-layer growth.

The present results encompass a wide range of somewhat contradictory previous observations. Konrad (1976), Jimenez (1983), and Bernal & Roshko (1986) have reported that the spanwise disturbance wavelength increased in a stepwise fashion with increasing streamwise distance. The results of Jimenez *et al.* (1985), Ho *et al.* (1988) and Huang & Ho (1990) strongly suggest that the spanwise wavelength increases during spanwise vortex pairing. Although the pairing locations are not fixed in the present (unforced) mixing layer, estimates of pairing locations using Ho & Huerre's (1984) scaling criterion are approximately consistent with the locations of the spanwise wavelength jumps. It has also been reported (Jimenez 1983; Bernal & Roshko 1986) that, on average, the spanwise wavelength increases linearly, at the same rate as the vorticity thickness. This is also the case in the present study, since linear least-squares fits show that the growth rate of the disturbance wavelength (twice the vortex spacing) is within about 6% of that of the vorticity thickness. In the region where the vortices have realigned into counter-rotating pairs ($X \geqslant 37$ cm), the ratio of twice the vortex spacing to the vorticity thickness is $2s/\delta_\omega = 1.28 \pm 0.21$, which agrees extremely well with the wavelength measurements of Jimenez ($\Lambda/\delta_\omega = 1$–$1.25$) and is comparable to the value determined from flow visualization by Bernal & Roshko ($\Lambda/\delta_\omega = 0.80 \pm 0.14$). The present results also show that the spanwise spacing can be constant over fairly large streamwise distances (up to 50 cm, or $450\theta_0$). This suggests that the results of Breidenthal (1978) and Lasheras *et al.* (1986), who reported no change in spacing with streamwise distance, may have been affected by this stepwise behaviour – their observations were perhaps not continued over a large enough streamwise distance to show the stepwise increasing trend. Another possible explanation was brought up by Huang & Ho (1990), who in their spectra of the mean velocity disturbances, found that the peak due to the initial (shorter) wavelength was slow to decay after vortex pairing, although a new higher wavelength peak had appeared. This raises the possibility that some measurement schemes may suffer from contamination due to the persistence of the initial wavelength.

A final point concerns a possible relationship between streamwise vortex spacing and circulation. The spacing data clearly show that the number of streamwise vortices is halved over a relatively short distance between the $X = 37$ cm and $X = 57$ cm stations. Figure 12 shows that an increase in the average vortex circulation occurs over the same distance. This suggests that it is some vortex amalgamation process which reduces the number of vortices, while increasing their circulation. The vorticity contour plots for the two relevant stations (figures 2*c* and 2*d*), show that the vortices are arranged in a single, more-or-less orderly row at both locations. Clearly, in order for vortex amalgamation to take place, a pair of opposite-signed vortices must rotate around each other so as to bring two like-signed vortices into closer contact. Such a rotation can take place between opposite-signed vortices if one vortex is significantly stronger than the other. The current data show a greater variation in circulation between vortices at the $X = 37$ cm station than at either of the two adjacent stations, suggesting that there is a greater tendency for vortices at this station to rotate out of the single row. This conjecture is supported by some recent results of a direct numerical simulation of a temporally developing mixing

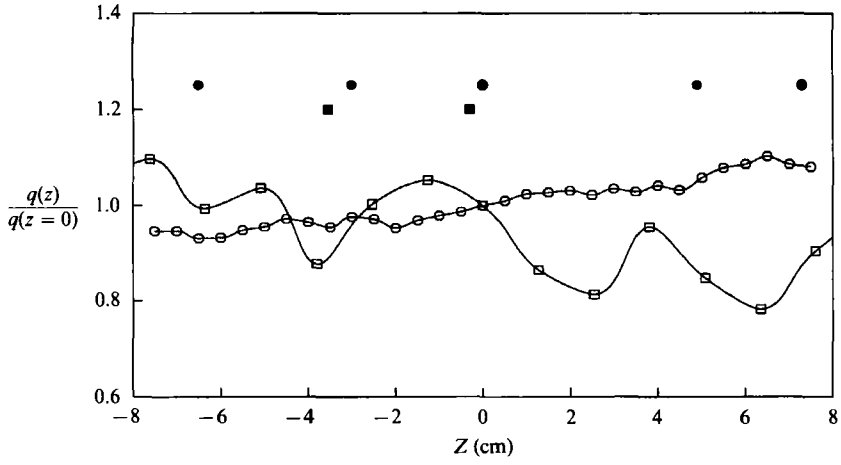

FIGURE 14. Spanwise variation of surface dynamic pressure on the splitter plate. Data are taken 0.4 cm upstream of the trailing edge: □, high-speed side; ○, low-speed side; ■, vortex cluster centres, $X = 8$ cm; ●, vortex cluster centres, $X = 17$ cm.

layer by Moser & Rogers (1990). Their simulations show both streamwise vortex amalgamation and annihilation occurring due to the interaction of unequal-strength vortices.

4.2. *Formation and reorganization of streamwise vorticity*

4.2.1. *Dependence on initial conditions*

Jimenez (1983) and Lasheras & Choi (1988) have reported that the spanwise location at which the streamwise vortices first appear is affected by small disturbances present in the incoming flow. They noted that the initial distribution of vortices in their facilities changed (but did not vanish) when attempts were made to clean up the incoming flow. In their analytic study of the initial formation of the streamwise vorticity, Corcos & Lin (1984) suggested that infinitesimally small upstream disturbances would be sufficient to initiate the formation process. In the present mean streamwise vorticity data, two distinct clusters can be seen at the first station ($X = 8$ cm), and five at the expanded second station ($X = 17$ cm). At $X = 8$ cm, the two clusters are located approximately 3.4 cm apart and at $X = 17$ cm, the five clusters are located at an average spacing of 3.3 cm. The clusters at $X = 8$ cm are still identifiable at $X = 17$ cm, but they appear to have shifted about 0.6 cm in the positive spanwise direction between the two stations. If the secondary vortex structure is indeed triggered by upstream disturbances, we would expect to find a corresponding spanwise wavelength in the disturbance field upstream of the splitter plate. Many sources exist for such small disturbances such as, for example, free-stream turbulence, mean velocity non-uniformity, and surface imperfections on the splitter plate.

On examining the splitter plate and upstream flow conditions no obvious non-uniformities were noted. The initial boundary layers also appeared to be adequately two-dimensional when the spanwise thickness and integral properties were examined. A more sensitive parameter for assessing boundary layer two-dimensionality, though, is the spanwise distribution of the skin friction coefficient (Bradshaw 1965). The surface dynamic pressure, q_0 (which is proportional to C_f^2 for a laminar boundary layer), measured on both sides of the splitter plate is shown in figure 14. Also shown in this figure are the locations of the vortex cluster centres at the first two stations. The variation on the high-speed side has a quasi-periodic character whereas that on

the low-speed side is much smaller in magnitude and free of any distinct wavelength. The spanwise variation in q_0 is attributed to the presence of weak streamwise vorticity which is strongly affected by upstream conditions, in particular the last screen in the wind tunnel settling chamber (Mehta & Hoffmann 1987). A peak in the surface pressure would then be associated with a pair of vortices with the common flow towards the surface, and vice versa.

The average spacing between clusters is quite close to the spacing of extrema in the surface pressure distribution measured on the high-speed side of the splitter plate. Within the range $Z = \pm 8$ cm, the average spacing between extrema of the q_0 distribution is about 2.6 cm. If the cluster centres identified at the second station are shifted in the negative spanwise direction, to counteract the apparent shift between the first and second stations, fairly good correspondence is noted between the adjusted centroid locations and the extrema in the q_0 distribution. So, as far as the position of the initial clusters is concerned, it appears as though it may be determined by the distribution of the skin friction coefficient in the initial boundary layer. It is not clear at this point if it will always be the high-speed side boundary layer, rather than one with the higher surface shear stress variation, that will determine the initial cluster positions.

In the light of this, the close match between the vortex spacing and the Kelvin–Helmholtz wavelength in the present case must be seen as somewhat fortuitous. It is worth noting that the cluster spacing is equivalent to only about twice the Kelvin–Helmholtz wavelength and Lasheras *et al.* (1986) have shown that (at least at low Reynolds numbers) the mixing layer will amplify a broad spectrum of spanwise disturbance wavelengths centred around the Kelvin–Helmholtz wavelength. So it seems as though any background disturbance in the facility that has a wavelength which is comparable to the Kelvin–Helmholtz wavelength will tend to get amplified.

4.2.2. *Initial formation of streamwise vorticity*

Measurements of frequency spectra in the near field indicate that the first spanwise vortex roll-up occurs at $X \sim 5$ cm. Mean velocity measurements made with a miniature Pitot tube indicate that the spanwise variation in U first becomes noticeable just downstream of $X = 5$ cm. Since the wrinkles in the mean velocity contours are caused by streamwise vorticity, this indicates that concentrated streamwise vortices first form just downstream of $X = 5$ cm ($X/\theta_0 = 44$), suggesting that the formation of the streamwise vortices is most probably caused by the braid instability, in agreement with many previous analyses (Jimenez *et al.* 1985; Bernal & Roshko 1986; Lasheras *et al.* 1986).

The pattern of streamwise vortices observed at the first measurement station bears little resemblance to that seen farther downstream. At the first station (figure 2*a*), the streamwise vortices appear to be grouped in isolated clusters, with each cluster containing three vortices aligned vertically across the mixing layer. In each cluster, two vortices of like sign flank a third, more flattened vortex of opposite sign. As noted previously, the two flanking vortices in each cluster are at the edges of the mixing layer, in the sense that the location of the peak vorticity is outside the region where $0.1 < U^* < 0.9$. It is interesting to speculate on the origins of this vortex cluster configuration. As discussed in the previous section, the initial distribution of vorticity in the mixing layer is approximately correlated with the spanwise variation of C_f on the high-speed side of the splitter plate. This is attributed to the presence of pairs of weak, counter-rotating streamwise vortices embedded in the boundary

layer. These weak vortices enter the mixing layer and presumably provide the background perturbation which the instability amplifies. The theoretical development of weak, diffuse streamwise vorticity in a plane strain field was examined by Lin & Corcos (1984). They found that streamwise vorticity first appeared in the form of flattened, diffuse vortices, which after some time rolled up, due to self-induction, into well-separated round structures. Lin & Corcos examined only the case of a regular initial distribution of streamwise vorticity, whereas the present data show that the actual vorticity distribution is very irregular. In regions where the initial triggering vorticity is relatively strong, the vortex formation process described by Lin & Corcos will be accelerated. The resultant distribution of streamwise vorticity might then include pairs of concentrated vortices (the stretched boundary-layer vortices) separated by diffuse vortices (where no triggering from the boundary layer has occurred) which have yet to roll up. The pairs of concentrated vortices would tend to rotate about each other, due to mutual induction, thus moving the individual vortices to the edges of the mixing layer. The resulting interaction between the concentrated and diffuse streamwise vortices would be complex, and could result in the three-vortex clusters observed at the first measurement station.

It is also possible that in the present time-averaged measurements the initial cluster does not represent three distinct structures, but just one. Direct numerical simulations (Buell & Mansour 1989; Rogers & Moser 1989) show the streamwise vortices in the braid region (rib vortices) being wrapped around the spanwise vortex cores, such that opposite-sign streamwise vorticity is generated in the core. Thus, a cross-sectional cut through a spanwise vortex core will show a cluster-type distribution, consisting of a central region of streamwise (core) vorticity, flanked by regions of opposite-sign (rib) vorticity. It is conceivable that the present measurements, averaged over several structures, would show a similar distribution, provided that the streamwise vorticity within and immediately flanking the spanwise vortex cores is much stronger than the streamwise vorticity in the braid region.

In either case, it is clear that the mixing-layer structure undergoes significant changes further downstream since the clusters are not maintained; an unravelling process takes place as discussed below.

4.2.3. *Reorganization of streamwise vorticity*

Streamwise vorticity is first observed in the form of clusters of vortices of unequal strength and scale. This configuration is not stable, and should reorganize due, at least partly, to inviscid vortex dynamics. Intuitively, it is expected that the reorganization will produce a single row of alternating sign vortices of roughly equal scale and strength, and this indeed occurs downstream of $X = 17$ cm. Although the mutual induction of the vortices is the most likely explanation for the reorganization, a closer look at vorticity transport in the mixing layer shows other processes at work, as well. The mean vorticity transport equation in a thin shear layer takes the form

$$U\frac{\partial \Omega_x}{\partial x}+V\frac{\partial \Omega_x}{\partial y}+W\frac{\partial \Omega_x}{\partial z}=\nu\left(\frac{\partial^2}{\partial y^2}+\frac{\partial^2}{\partial z^2}\right)\Omega_x+\underbrace{\Omega_x\frac{\partial U}{\partial x}-\frac{\partial U}{\partial y}\frac{\partial W}{\partial x}+\frac{\partial U}{\partial z}\frac{\partial V}{\partial x}}_{P_1}$$
$$+\underbrace{\frac{\partial^2}{\partial y\,\partial z}\left(\overline{v'^2}-\overline{w'^2}\right)}_{P_2}+\underbrace{\left(\frac{\partial^2}{\partial x^2}-\frac{\partial^2}{\partial y^2}\right)\overline{v'w'}}_{P_3}. \quad (8)$$

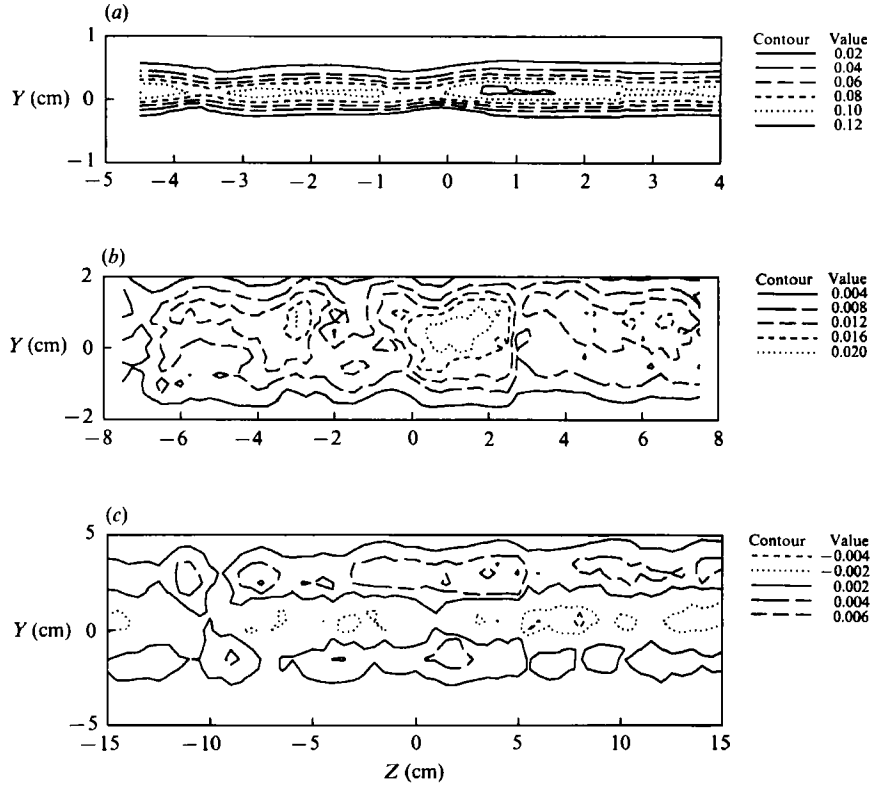

FIGURE 15. Normal-stress anisotropy ($(\overline{v'^2}-\overline{w'^2})/U_0^2$) contours: (*a*) $X = 8$ cm; (*b*) 37 cm; (*c*) 78 cm.

The following discussion closely follows the analysis of Wood (1982), who obtained a theoretical relation for the decay rate of streamwise vorticity in a mixing layer. Wood showed, through a relatively simple order-of-magnitude analysis, that the terms P_1 and P_3 are negligible compared to P_2, which is thus the only significant production term. The cross-flow normal stresses, $\overline{v'^2}$ and $\overline{w'^2}$, are roughly equal in a self-similar (two-dimensional) mixing layer, and Wood therefore assumed that P_2 was also negligible. When the vorticity transport equation is integrated under these conditions, it is found that streamwise vorticity decays as $1/X^2$. However, a non-zero level of P_2 will cause some production of streamwise vorticity, resulting in a decay rate slower than $1/X^2$. In the near field of the mixing layer, $\overline{v'^2}$ is typically much larger than $\overline{w'^2}$, and so it might be expected that higher levels of streamwise vorticity will be found preferentially in regions where P_2 was high. The behaviour of P_2 is difficult to assess directly, since taking the second derivative of experimental data is a notoriously unreliable process. Accordingly, the behaviour of the normal-stress anisotropy ($\overline{v'^2}-\overline{w'^2}$) is examined here instead at three streamwise locations (figure 15*a–c*). Saddle points in $\overline{v'^2}-\overline{w'^2}$ oriented at 45° to the Y- and Z- axes would correspond to peaks in the P_2 distribution.

The relative levels of $\overline{v'^2}$ and $\overline{w'^2}$ change considerably as the mixing layer develops, changing the distribution of P_2. At the upstream stations, $\overline{v'^2}$ is much larger than $\overline{w'^2}$, and as a result the $\overline{v'^2}-\overline{w'^2}$ distribution is fairly simple and symmetric around the centreline as seen in figure 15(*a*). The cross-stream gradient of $\overline{v'^2}-\overline{w'^2}$ is zero along the mixing-layer centreline, and rises to a high level toward the edges. Spanwise

gradients of $\overline{v'^2}-\overline{w'^2}$ are approximately equal at both the edges and centreline of the mixing layer. The symmetric distribution results in a low level of P_2 at the centre of the layer, relative to the edges. Accordingly, the decay rate of mean streamwise vorticity should be higher at the centre of the mixing layer compared to the edges. As the flow evolves downstream, $\overline{v'^2}$ drops with respect to $\overline{w'^2}$, the two quantities become more equal (figure 15*b*), and the result is a more complex distribution of $\overline{v'^2}-\overline{w'^2}$ in the centre of the mixing layer. Thus, gradients of $\overline{v'^2}-\overline{w'^2}$ within the mixing layer are increased with respect to gradients at the edges. Now both the centre and edges of the mixing layer have equal rates of mean vorticity decay. By the $X = 78$ cm station (figure 15*c*), the $\overline{v'^2}$ peak level has decreased below the $\overline{w'^2}$ peak level. Since the $\overline{v'^2}$ distribution is wider, however, the resulting $\overline{v'^2}-\overline{w'^2}$ distribution shows a negative region running along the mixing-layer centreline, flanked by peaks of positive $\overline{v'^2}-\overline{w'^2}$. The resulting distribution of P_2 would tend to maintain streamwise vorticity along the mixing-layer centreline.

On the whole, the location of the streamwise vortices is consistent with the behaviour of the normal stress anisotropy. At the first two stations, the majority of the vortices are found along the edges of the mixing layer, while further downstream, the vortices occur mostly on the centreline.

4.3. *Downstream development of streamwise vorticity*

4.3.1. *Persistence into the far-field region*

Organized streamwise vorticity is found to persist into the far-field region of the mixing layer, as shown in figure 2(*a–i*), although the mean vorticity levels continue to decrease with downstream distance. By conventional criteria, the mixing layer appears to be self-similar beyond $X = 100$ cm ($X = 880\theta_0$), as discussed above in §3.3. At $X = 108$ cm, average peak streamwise vorticity is 0.026 cm^{-1}, which is only 4% of the measured level at the first station, and 14% of the estimated peak spanwise vorticity at this station. Nonetheless, organized streamwise vortices are still visible in contour plots at this station, and can be observed all the way to the $X = 189$ cm station, almost twice the distance at which self-similarity appeared to have been achieved. Only at the last station ($X = 250$ cm) is the pattern of vorticity totally lost amongst the measurement noise, although even at this station, definite peaks in the $\overline{u'w'}$ distribution (which is strongly correlated with Ω_x) can be seen. Therefore, the accepted criteria for the achievement of self-similarity may need to be re-evaluated when significant streamwise vorticity exists in the layer. A criterion based on parameters, such as $\overline{u'w'}$, which accounts for the three-dimensional nature of the mixing layer should also be included (Bell & Mehta 1990*b*).

4.3.2 *Possible meander of the streamwise vortices*

Bushnell (1984) suggested that streamwise vortices in wall-bounded flows may fluctuate bodily or 'meander', and it has been proposed that the streamwise vortices found in mixing layers also behave in this fashion. To the extent that the vortices meander, instantaneous and time-averaged measurements of vorticity will differ, in exactly the same way that a long-time-exposure photograph of a moving object is blurred in comparison with a short-time-exposure photograph. All the vorticity data in the current study were obtained by differentiating single-point, time-averaged velocity measurements. The averaging time (12.5 s) was large compared to all characteristic timescales in the flow, so the present results are subject to the effect described above. The appearance of meandering vortices on a mean vorticity contour plot is easily anticipated; if the amplitude of the meander is low relative to the radius

of the vortices, they will appear larger, and their effective peak vorticity will be lowered. If the meander amplitude is larger than the vortex spacing, adjacent opposite-sign vortices will cancel each other out, drastically reducing the measured mean vorticity. Lateral meander of the secondary vortex structure has been reported previously by Bernal & Roshko (1986), on the basis of their still photographs and a motion picture. They estimated that the meander began, approximately, at the end of mixing transition, as determined by concentration measurements. The amplitude of the meander increased with streamwise distance until the streamwise vortices were totally obscured.

These observations suggest the possibility that the steady decrease in mean vortex strength seen in the present experiment is not due to the decay of the vortices themselves, but results when vortices of constant strength meander with increasing amplitude as they move downstream. While the present measurements cannot immediately distinguish between these two alternatives, a close examination of the present data reveals some reasons for believing that the postulated lateral meander of the vortices is not occurring in this case.

Low-amplitude lateral meander should effectively elongate the vortex in the spanwise direction, as discussed above. This behaviour has been shown to occur in a study of a streamwise vortex which was deliberately made to oscillate laterally in a boundary layer (Westphal & Mehta 1989). Vortices flattened in the lateral direction are very rarely observed in the contour plots of the present study. In fact, if anything, more of the vortices tend to be elongated in the cross-stream direction, the implications of which are discussed below. Another argument against the possibility of lateral vortex meander can be made from the effect of the streamwise vorticity on the Reynolds stress distributions. Westphal & Mehta (1989) showed that when a streamwise vortex embedded in a boundary layer is made to meander, its measured peak vorticity decreases, but Reynolds stresses are increased in the region of the vortex. The cross-stream normal stress ($\overline{v'^2}$) is the most markedly affected, as would be expected, since V changes sign across the vortex in the lateral direction. In fact, normal stresses can be increased by up to a factor of two when a fairly strong vortex meanders in the boundary layer. There is also a characteristic qualitative change in the distribution of the Reynolds stresses associated with the meandering vortex. It seems reasonable to suppose that meandering vortices in a mixing layer will leave a similar 'footprint' in the form of increased cross-stream stresses at the vortex locations. However, no such behaviour is observed in the present case.

In an earlier prototype study (Bell & Mehta 1990*a*), a single streamwise vortex was made to interact with a single-stream mixing layer originating from a turbulent initial boundary layer. Measurements were obtained and compared for the cases with and without the artificially induced vortex present. The induced vortex was found to decay with downstream distance, to a point where the vortex was no longer discernable in the mean vorticity plots. However, it should still be possible to detect the presence of the vortex, if its 'decay' was actually due to meander, since an increased $\overline{v'^2}$ should be observed relative to the case without the vortex. Such a 'footprint' was not noted, suggesting that vortex meander was not responsible for the observed decay. By the same token, we believe that the decay of the streamwise vortices observed in the present study is not caused by lateral meander.

It is important to distinguish between effects due to meander, and those due to the angle the secondary vortex structure makes with the mean flow. According to the current model of the secondary vortex structure, the vortices wind over and under adjacent spanwise vortices, making an angle with the streamwise direction. As a

result, a stationary observer looking upstream into the mixing layer will see streamwise vortices 'meandering' in the *cross-stream* direction with an amplitude roughly equal to the mixing-layer thickness. Time-averaged measurements will show a vorticity distribution which is elongated in the cross-stream direction, and, as suggested by the results of Westphal & Mehta (1989), there will be an increase in $\overline{w'^2}$ at the vortex locations. Both the vortex elongation and the increase in $\overline{w'^2}$ are observed in the present data, which is consistent with the current model of the secondary structure.

So although the question of vortex meander cannot be fully resolved from the present measurements, the balance of evidence suggests that most of the observed streamwise vorticity decay is real, rather than an artifact of Reynolds averaging in the presence of vortex meander.

4.4. *Effect of streamwise vorticity on Reynolds stresses*

The presence of streamwise vorticity is found to affect both the mean flow and turbulence properties of the mixing layer. The first effect of the vortices is to directly modify the momentum transport such that a peak is produced in the region of upwash and vice versa. This effect is responsible for the wrinkles seen in the mean velocity contour plots (figures 3 and 4). Streamwise vorticity also affects the mean velocity gradients since $\partial U/\partial Z$ is generated within the mixing layer while the spanwise distribution of $\partial U/\partial Y$ is altered. Secondary mean velocities (V and W), and gradients thereof, are also obviously generated by the presence of the streamwise vorticity. As a result, production of the Reynolds stresses is affected. For example, the main production term for the primary shear stress ($\overline{u'v'}$) is $\overline{v'^2}\,\partial U/\partial Y$; since $\partial U/\partial Y$ now varies across the mixing-layer span, local peaks and wrinkles are observed in the contour plots of $\overline{u'v'}$. The production and distribution of the turbulent kinetic energy is also affected by the altered mean velocity gradient distribution.

The component of the Reynolds stress tensor most profoundly affected by the streamwise vorticity is the secondary shear stress, $\overline{u'w'}$. The present study shows that peaks in $\overline{u'w'}$ are associated with identically signed peaks in the streamwise vorticity. The connection between the two quantities can be seen by examining the transport equation for $\overline{u'w'}$. Neglecting variation in X, triple products, pressure variation, and viscous terms, the equation can be written in the following simplified form:

$$\frac{\mathrm{D}}{\mathrm{D}t}(\overline{u'w'}) = \underbrace{-\overline{w'^2}\frac{\partial U}{\partial z}}_{P_1} \underbrace{-\overline{u'w'}\frac{\partial W}{\partial z}}_{P_2} \underbrace{-\overline{u'v'}\frac{\partial W}{\partial y}}_{P_3} \underbrace{-\overline{v'w'}\frac{\partial U}{\partial y}}_{P_4}. \tag{9}$$

All four production terms on the right-hand side are approximately zero in a nominally two-dimensional mixing layer, which does not contain noticeable spanwise variation or secondary flows. In the presence of streamwise vorticity, these terms become significant and take on a distribution which is associated with the vorticity. Out of the four, the first three terms can be evaluated from the present measurements. The term P_1 becomes significant when streamwise vorticity distorts the mixing-layer mean streamwise velocity contours. This distortion of the shear layer produces a peak in $\partial U/\partial z$ at the location of each vortex, which in turn produces a peak in P_1. The association of P_2 and P_3 with the vortex can be seen by modelling each streamwise vortex as a simple Rankine vortex and calculating the $\partial W/\partial z$ and $\partial W/\partial y$ cross-flow gradients. It is seen that each term generates a quartet of peaks, two positive and two negative, clustered around the position of each vortex core. While P_4 contains the

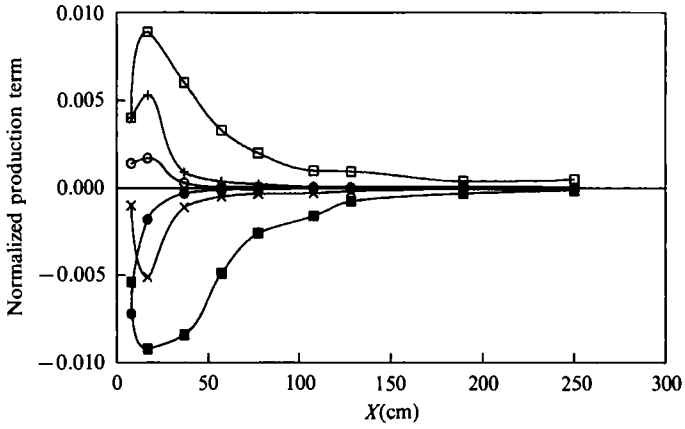

FIGURE 16. Relative magnitudes and streamwise evolution of $\overline{u'w'}$ production terms (equation (9)): □, peak positive P_1; ■, peak negative P_1; ○, peak positive P_2; ●, peak negative P_2; +, peak positive P_3; × peak negative P_3.

relatively large $\partial U/\partial y$ term, it is also dependent on $\overline{v'w'}$. While this stress was not measured in the present study, it was measured in the vortex/mixing-layer experiment (Bell & Mehta 1990*a*) and the results indicated that $\overline{v'w'}$ is likely to be relatively small in the present study.

Contour plots of the production terms (not presented here) show that at the upstream locations, there is no strong resemblance between the distributions of P_1, P_2, or P_3 and those of either $\overline{u'w'}$ or streamwise vorticity. Thus, either no one term dominates the $\overline{u'w'}$ production, or there is a substantial contribution from P_4. On the other hand, further downstream (beyond $X = 37$ cm), P_1 dominates the other production terms, and, in addition, the distribution of P_1 corresponds very closely with that of $\overline{u'w'}$. Further evidence that P_1 is the dominant production term is given in figure 16, in which the peak positive and negative values of the three measured production terms are plotted as functions of the streamwise distance. All three production terms increase between the first and second stations, and then drop with increasing streamwise distance. Initially, the production terms are comparable, but P_2 and P_3 decrease much more rapidly than P_1, leaving it as the dominant production term past $X = 37$ cm.

The correlation between the $\overline{u'w'}$ and streamwise vorticity distributions is quite striking. At all but the first two stations, the contour plots of streamwise vorticity and $\overline{u'w'}$ compare very favourably. The correlation between $\overline{u'w'}$ and streamwise vorticity extends to relative strengths as well. This can be seen by dividing the average peak vorticity by the average peak $\overline{u'w'}$, and plotting the ratio against streamwise distance (figure 17). It is interesting to note that the ratio reaches a more-or-less constant value beyond $X \sim 50$ cm. As shown above, the peaks of $\overline{u'w'}$ are due to peaks in the first production term, $P_1 = \overline{w'^2}(\partial U/\partial z)$. Since spanwise variation in $\overline{w'^2}$ is less than 20% at the downstream stations, it is actually the peaks in $\partial U/\partial z$ that are responsible for the observed distribution of $\overline{u'w'}$. This derivative is the dominant component of the *cross-stream* vorticity, $\Omega_y = (\partial U/\partial z) - (\partial W/\partial x)$, so, in reality, $\overline{u'w'}$ is associated with Ω_y, and peak Ω_y is associated with peak Ω_x. The constant ratio of $\overline{u'w'}$ to Ω_x implies that the vortex structures maintain a constant angle with the streamwise direction.

Since the distributions of $\overline{u'w'}$ and Ω_x are well-correlated, $\overline{u'w'}$ can be used as an indicator for the presence of streamwise vorticity. In order to measure Ω_x, two passes

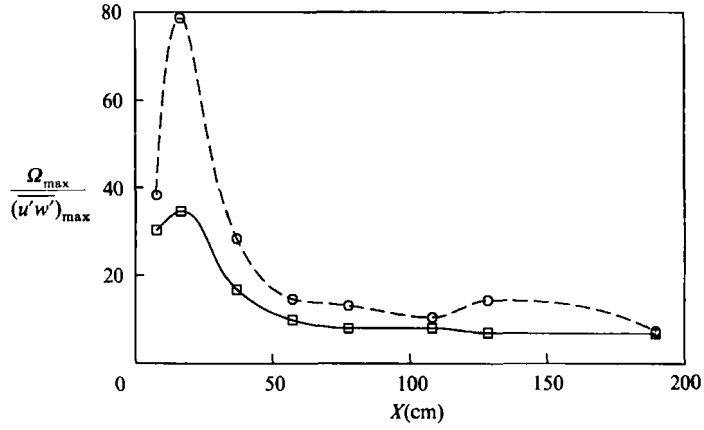

FIGURE 17. Streamwise evolution of the ratio of streamwise vorticity to secondary shear stress: □, positive; ○, ABS (negative).

must be made through the flow with the cross-wire probe, and the secondary velocity data must then be differentiated and subtracted. In contrast, $\overline{u'w'}$ is measured directly with only a single pass through the flow. The higher sensitivity of the $\overline{u'w'}$ data to the secondary vortex structure is indicated by the fact that, in the region where a regular array of vortices is established, the $\overline{u'w'}$ data appear a lot 'cleaner', with a peak in $\overline{u'w'}$ often observed when the corresponding vorticity contours are missing – this is clearly seen by comparing corresponding stations in figures 2 and 8. This means that the scale and, to some extent, the strength of streamwise vorticity in shear flows can be quickly determined through the $\overline{u'w'}$ measurements. Lastly, it should be noted that the peak levels of $\overline{u'w'}$ are comparable to those of $\overline{u'v'}$ and this, together with the well-developed distribution of $\overline{u'w'}$, indicates that this quantity is significant to the development of mixing layers. Thus, the $\overline{u'w'}$ distribution must be modelled correctly if simulations of the Reynolds-averaged Navier–Stokes equations are to accurately compute mixing layers developing from laminar initial boundary layers.

5. Conclusions

Measurements have been made of the streamwise vortex structure in a plane two-stream mixing layer of velocity ratio 0.6 and originating from laminar initial boundary layers. The results obtained in the present study allow several conclusions to be drawn concerning both mixing-layer behaviour in general and the development of streamwise vorticity in mixing layers in particular.

5.1. *Origin of streamwise vorticity in mixing layers*

The formation of the streamwise vortex structure is triggered by very small (spatial) disturbances present in the mixing layer. Sufficiently strong disturbances can be found even in flows which are generally regarded to be 'clean' or two-dimensional. In the present study, the disturbances are believed to occur in the form of weak streamwise vortices originating in the upstream boundary layer. The streamwise vortex structure begins to form just downstream of the first spanwise vortex roll-up. The data tend to support the conclusion that the streamwise vortices are produced through a braid instability, rather than the deformation of the spanwise vortex

cores. Streamwise vortices initially appear grouped in clusters of three. In each cluster, a central, diffuse vortex is flanked by two vortices of opposite sign, positioned towards the outer edges of the mixing layer. The details of this formation may depend on the nature and distribution of the triggering disturbances. The disturbance whose wavelength is comparable to the Kelvin–Helmholtz wavelength is most likely to get amplified. The initial average peak streamwise vorticity is about 30% of the initial Kelvin–Helmholtz spanwise vorticity, and the average streamwise vortex circulation is about 10% of the spanwise vortex circulation.

5.2. *Evolution of streamwise vorticity in mixing layers*

The initial vortex clusters unwrap to form a single row of alternating-sign streamwise vortices embedded in the mixing layer. This reorganization process, while driven by the inviscid interaction of the vortices, is also found to be consistent with changes in the normal stress anisotropy parameter. The average peak streamwise vorticity decreases as approximately $1/X^{1.5}$, somewhat slower than the $1/X^2$ decay expected for an isolated vortex in a self-similar mixing layer. The difference in decay rates is most likely due to interactions between the individual streamwise vortices, and to changes in the normal-stress anisotropy associated with the evolution of the mixing layer. Note that, in general, the decay rate may also be a function of velocity ratio. Although peak vorticity changes by more than an order of magnitude as the mixing layer evolves, the mean streamwise vortex circulation remains more or less constant. The average streamwise vortex spacing increases in a nonlinear (stepwise) fashion. The *overall* vortex spacing scales approximately with the mixing-layer vorticity thickness. A factor-of-two jump in the streamwise vortex spacing appears to be due to the amalgamation of like-sign vortices, since the average circulation also jumps at the same streamwise location.

5.3. *Persistence of streamwise vorticity into the far-field region*

Extensive measurements show that the present mixing layer meets all the *conventional* criteria for the attainment of a self-similar state by a plane mixing layer. A linear growth rate is achieved and the Reynolds-normal-stress peaks, as well as the primary-shear-stress peak, asymptote to constant levels. Organized streamwise vorticity is measured in the 'self-similar' region, although it continues to decay throughout the region of measurement, without reaching an asymptotic state. The observed decrease in peak vorticity seems to represent actual vortex decay, rather than the effects of vortex meander, although the present results are by no means conclusive. The persistence of streamwise vorticity into the 'self-similar' region suggests that the current criteria for self-similarity may need to be re-assessed.

5.4. *Effect of streamwise vorticity on mixing-layer properties*

The streamwise vortex structure generates a pattern of wrinkles in the mean streamwise velocity contours. The wavelength and amplitude of the wrinkles are determined by the spacing, strength, and pattern of the streamwise vortices. New gradients in the mean velocities produced by the streamwise vortex structure generate 'extra' production of the Reynolds stresses. The resulting stress distributions have a pattern of wrinkles similar to that of the mean velocity distribution, but with the addition of localized peaks along the mixing-layer centreline. Spanwise variations of up to 40% in the peak Reynolds stresses are observed in the near field. This can be a significant source of scatter in near-field measurements of mixing layers if these are based on only a single profile measured

across the layer. The distribution of the secondary shear stress, $\overline{u'w'}$, is strongly correlated, in both position and strength, with the distribution of streamwise vorticity. Since $\overline{u'w'}$ is generally easier to measure than streamwise vorticity, the distribution of $\overline{u'w'}$ serves as a very useful indicator of streamwise vorticity in mixing layers. The effect of streamwise vorticity on the near-field behaviour of the mixing layer is sufficiently strong that the streamwise vortex structure should be included in all modelling of mixing layers originating from laminar initial boundary layers.

This work was supported by and conducted in the Fluid Mechanics Laboratory, Fluid Dynamics Research Branch, NASA Ames Research Center, California under Grant NCC-2-55 monitored by Dr S. S. Davis. We are grateful to Professors L. Roberts, B. J. Cantwell, J. K. Eaton and P. Bradshaw of Stanford University for helpful discussions and comments.

REFERENCES

ABRAMOVICH, G. N. 1963 *The Theory of Turbulent Jets*. MIT Press.

ANDERSEN, N. 1974 On the calculation of filter coefficients for maximum entropy spectral analysis. *Geophys.* **39**, 69–72.

ASHURST, W. T. & MEIBURG, E. 1988 Three-dimensional shear layers via vortex dynamics. *J. Fluid Mech.* **189**, 87–116.

BELL, J. H. & MEHTA, R. D. 1989*a* Three-dimensional structure of plane mixing layers. *JIAA Rep.* TR-90. Dept. of Aeronautics and Astronautics, Stanford University.

BELL, J. H. & MEHTA, R. D. 1989*b* Design and calibration of the mixing layer wind tunnel. *JIAA Rep.* TR-89. Dept. of Aeronautics and Astronautics, Stanford University.

BELL, J. H. & MEHTA, R. D. 1990*a* Interaction of a streamwise vortex with a turbulent mixing layer. *Phys. Fluids* A **2**, 2011–2023.

BELL, J. H. & MEHTA, R. D. 1990*b* Development of a two-stream mixing layer with tripped and untripped boundary layers. *AIAA J.* **28**, 2034–2042.

BERNAL, L. P. 1981 The coherent structure of turbulent mixing layers. Ph.D. thesis, California Institute of Technology.

BERNAL, L. P. & ROSHKO, A. 1986 Streamwise vortex structure in plane mixing layers. *J. Fluid Mech.* **170**, 499–525.

BIRCH, S. F. 1981 Planar mixing layer. In *AFOSR-HTTM-Stanford Conf. on Complex Turbulent Flows* (ed. S. J. Kline, B. J. Cantwell & G. M. Lilley), vol. 1, pp. 170–175.

BRADSHAW, P. 1965 The effect of wind tunnel screens on nominally two-dimensional boundary layers. *J. Fluid Mech.* **22**, 679–687.

BRADSHAW, P. 1966 The effect of initial conditions on the development of a free shear layer. *J. Fluid Mech.* **26**, 225–236.

BRADSHAW, P. 1979 Introduction to the section on 'Coherent Structures'. In *Turbulent Shear Flows 2* (ed. L. J. S. Bradbury, F. Durst, B. E. Launder, F. W. Schmidt & J. H. Whitelaw), vol. 2, pp. 259–262. Springer.

BRADSHAW, P., FERRISS, D. H. & JOHNSON, R. F. 1964 Turbulence in the noise producing region of a circular jet. *J. Fluid Mech.* **19**, 591–624.

BREIDENTHAL, R. 1978 A chemically reacting plane shear layer. Ph.D. thesis, California Institute of Technology (Aero 105–50).

BREIDENTHAL, R. 1981 Structure in turbulent mixing layers and wakes using a chemical reaction. *J. Fluid Mech.* **109**, 1–24.

BROWAND, F. K. & TROUTT, T. R. 1985 The turbulent mixing layer: geometry of large vortices. *J. Fluid Mech.* **158**, 489–509.

BROWN, G. L. & ROSHKO, A. 1974 On density effects and large structure in turbulent mixing layers. *J. Fluid Mech.* **64**, 775–816.

BUELL, J. C. & MANSOUR, N. N. 1989 Asymmetric effects in three-dimensional spatially-developing mixing layers. In *Proc. Seventh Symp. on Turbulent Shear Flows, Stanford University, August*, pp. 9.2.1–9.2.6.

BUSHNELL, D. M. 1984 Body–turbulence interaction. *AIAA Paper* 84-1527, Presented at the *17th Fluid Dynamics, Plasma Physics, and Lasers Conf., Snowmass, Colorado, June 25–27.*

CANTWELL, B. J. 1981 Organized motion in turbulent flow. *Ann. Rev. Fluid Mech.* **13**, 457–515.

CHANDRSUDA, C., MEHTA, R. D., WEIR, A. D. & BRADSHAW, P. 1978 Effect of free-stream turbulence on large structure in turbulent mixing layers. *J. Fluid Mech.* **85**, 693–704.

CORCOS, G. M. & LIN, S. J. 1984 The mixing layer: deterministic models of a turbulent flow. Part 2. The origin of the three-dimensional motion. *J. Fluid Mech.* **139**, 67–95.

CORCOS, G. M. & SHERMAN, F. S. 1984 The mixing layer: deterministic models of a turbulent flow. Part 1. Introduction and the two-dimensional flow. *J. Fluid Mech.* **139**, 29–65.

FREYMUTH, P. 1966 On transition in a separated laminar boundary layer. *J. Fluid Mech.* **25**, 683–704.

HO, C.-M. & HUERRE, P. 1984 Perturbed free shear layers. *Ann. Rev. Fluid Mech.* **16**, 365–424.

HO, C.-M., ZOHAR, Y., MOSER, R. D., ROGERS, M. M., LELE, S. K. & BUELL, J. C. 1988 Phase decorrelation, streamwise vortices and acoustic radiation in mixing layers. *Center for Turbulence Research Rep.* CTR-88, pp. 29–39. Stanford University.

HUANG, L.-S. & HO, C.-M. 1990 Small-scale transition in a plane mixing layer. *J. Fluid Mech.* **210**, 475–500.

INOUE, O. 1987 Three-dimensional vortex simulation of a plane mixing layer. In *Proc. Sixth Symp. on Turbulent Shear Flows, Toulouse, France, September 7–9*, pp. 22-1-1 to 22-1-6.

JIMENEZ, J. 1983 A spanwise structure in the plane mixing layer. *J. Fluid Mech.* **132**, 319–326.

JIMENEZ, J., COGOLLOS, M. & BERNAL, L. P. 1985 A perspective view of the plane mixing layer. *J. Fluid Mech.* **152**, 125–143.

KONRAD, J. H. 1976 An experimental investigation of mixing in two-dimensional turbulent shear flows with applications to diffusion-limited chemical reactions. *Project SQUID Tech. Rep.* CIT-8-PU; and Ph.D. thesis, California Institute of Technology, 1977.

LASHERAS, J. C., CHO, J. S. & MAXWORTHY, T. 1986 On the origin and evolution of streamwise vortical structures in a plane, free shear layer. *J. Fluid Mech.* **172**, 231–258.

LASHERAS, J. C. & CHOI, H. 1988 Three-dimensional instability of a plane free shear layer: an experimental study of the formation and evolution of streamwise vortices. *J. Fluid Mech.* **189**, 53–86.

LIEPMANN, H. W. & LAUFER, J. 1947 Investigation of free turbulent mixing. NACA-TN 1257.

LIN, S. J. & CORCOS, G. M. 1984 The mixing layer: deterministic models of a turbulent flow. Part 3. The effect of plane strain on the dynamics of streamwise vortices. *J. Fluid Mech.* **141**, 139–178.

MARTEL, C., MORA, E. & JIMENEZ, J. 1989 Small-scales generation in 2-D mixing layers. *Bull. Am. Phys. Soc.* **34**, 2268.

MEHTA, R. D. 1991 Effect of velocity ratio on plane mixing layer development: influence of the splitter plate wake. *Exps Fluids* **10**, 194–204.

MEHTA, R. D. & HOFFMANN, P. H. 1987 Boundary layer two-dimensionality in wind tunnels. *Exps Fluids* **5**, 358–360.

MEHTA, R. D. & WESTPHAL, R. V. 1986 Near-field turbulence properties of single- and two-stream plane mixing layers. *Exps Fluids* **4**, 257–266.

METCALFE, R. W., ORSZAG, S. A., BRACHET, M. E., MENON, S. & RILEY, J. J. 1987 Secondary instability of a temporally growing mixing layer. *J. Fluid Mech.* **184**, 207–243.

MOSER, R. D. & ROGERS, M. M. 1990 Spanwise scale change in a time-developing mixing layer. *Bull. Am. Phys. Soc.* **35**, 2294.

NYGAARD, K. J. & GLEZER, A. 1990 Core instability of the spanwise vortices in a plane mixing layer. *Phys. Fluids* A **2**, 461–463.

O'HERN, T. J. 1990 An experimental investigation of turbulent shear flow cavitation. *J. Fluid Mech.* **215**, 365–391.

PIERREHUMBERT, R. T. & WIDNALL, S. E. 1982 The two- and three-dimensional instabilities of a spatially periodic shear layer. *J. Fluid Mech.* **114**, 59–82.

PLESNIAK, M. W. & JOHNSTON, J. P. 1989 The effects of longitudinal curvature on turbulent two-stream mixing layers. *Rep.* MD-54. Thermosciences Division, Dept. of Mechanical Engineering, Stanford University.

POLINSKY, D. I. 1989 Determinism and randomness in a two stream mixing layer. Ph.D. thesis, Dept. of Mechanical Engineering, University of California, Berkeley.

RODI, W. 1975 A review of experimental data of uniform density free turbulent boundary layers. In *Studies in Convection* (ed. B. E. Launder), vol. 1, pp. 79–165, Academic.

ROGERS, M. M. & MOSER, R. D. 1989 The development of three-dimensional temporally-evolving mixing layers. In *Proc. Seventh Symp. on Turbulent Shear Flows, Stanford University, August*, pp. 9.3.1–9.3.6.

SABIN, C. M. 1965 An analytical and experimental study of the plane, incompressible, turbulent free-shear layer with arbitrary velocity ratio and pressure gradient. *Trans. ASME* D: *J. Basic Engng* **87**, 421–428.

TOWNSEND, A. A. 1956 *Structure of Turbulent Shear Flow* (1st Edn). Cambridge University Press.

TOWNSEND, A. A. 1976 *Structure of Turbulent Shear Flow* (2nd Edn). Cambridge University Press.

WESTPHAL, R. V. & MEHTA, R. D. 1989 Interaction of an oscillating vortex with a turbulent boundary layer. *Exps Fluids* **7**, 405–411, 1989.

WINANT, C. D. & BROWAND, F. K. 1974 Vortex pairing: the mechanism of turbulent mixing layer growth at moderate Reynolds number. *J. Fluid Mech.* **63**, 237–255.

WOOD, D. H. 1982 Spanwise non-uniformities in a nominally plane mixing layer. *Tech. Note* FM 82/3. Dept. Mechanical Engng, University of Newcastle, Australia.